Entropy-Preserving and Entropy-Stable Relaxation IMEX and Multirate Time-Stepping Methods

Shinhoo Kang[a,*], Emil M. Constantinescu[a]

[a]*Mathematics and Computer Science Division, Argonne National Laboratory, Lemont, IL, USA*

Abstract

We propose entropy-preserving and entropy-stable partitioned Runge–Kutta (RK) methods. In particular, we extend the explicit relaxation Runge–Kutta methods to IMEX–RK methods and a class of explicit second-order multirate methods for stiff problems arising from scale-separable or grid-induced stiffness in a system. The proposed approaches not only mitigate system stiffness but also fully support entropy-preserving and entropy-stability properties at a discrete level. The key idea of the relaxation approach is to adjust the step completion with a relaxation parameter so that the time-adjusted solution satisfies the entropy condition at a discrete level. The relaxation parameter is computed by solving a scalar nonlinear equation at each timestep in general; however, as for a quadratic entropy function, we theoretically derive the explicit form of the relaxation parameter and numerically confirm that the relaxation parameter works the Burgers equation. Several numerical results for ordinary differential equations and the Burgers equation are presented to demonstrate the entropy-conserving/stable behavior of these methods. We also compare the relaxation approach and the incremental direction technique for the Burgers equation with and without a limiter in the presence of shocks.

Keywords: entropy conservation/stability, discontinuous Galerkin, implicit-explicit, multirate integrator, Burgers equation

1. Introduction

High-order methods for solving partial differential equations are popular because of their high-order accuracy and low numerical dissipation and dispersion errors, compared with low-order schemes [1]. In terms of numerical robustness, however, the low-order schemes are still an attractive choice for computational fluid dynamics because they are less prone to numerical instability than are

---

*Corresponding author

Email addresses: `shinhoo.kang@anl.gov` (Shinhoo Kang), `emconsta@anl.gov` (Emil M. Constantinescu)

high-order methods [2]. To this end, further stabilization techniques such as artificial viscosity, slope limiting, or filtering are needed in the vicinity of shocks or underresolved features.

The entropy-conserving and entropy-stable methods are an alternative way to improve robustness by satisfying the entropy condition at a discrete level. Tadmor [3] proposed entropy-conservative/stable finite-volume schemes, which are extended to high-order methods [4, 5, 6, 7, 8, 9, 10] with two important tools: the summation by parts (SBP) operator and flux-differencing techniques. [1] In particular, several entropy-stable discontinuous Galerkin (DG) methods have been developed with collocated points on quadrilateral and hexagonal meshes [11, 12], on triangular meshes [13], and with general points [2] by a hybridized SBP operator.

From a time discretization perspective, Nordström and Lundquist in [14] proposed SBP-based implicit time integrators to have fully discrete entropy-stable schemes. The work in [15, 16] incorporated SBP in implicit Runge–Kutta (RK) methods. Friedrich et al. [17] proposed entropy-stable space-time methods. For entropy-stable explicit time integrators, Ketcheson [18] modified the step completion in standard Runge–Kutta methods to guarantee the square entropy conservation or stability, namely, L^2 stability, which are referred to as relaxation methods. [2]

The relaxation idea stems from the earlier works of Sanz-Serna and Manoranjan [19, 20], which modified the time step size of the Leapfrog scheme for the *Korteweg–de Vries* equation and nonlinear *Schrödinger* equations such that the quadratic invariant is conserved at a fully discrete level. Ketcheson [18] revisited this relaxation idea and developed relaxation Runge–Kutta methods that guarantee conservation or stability for any inner-product norm. Relaxation methods have been further extended to the multistep methods [21] and deferred correction methods [22] and studied for Hamiltonian problems [23], compressible Euler, and Navier–Stokes equations [24].

Inspired by the work in [18], we propose the relaxation methods for partitioned RK methods to tackle stiff problems. Specifically, we extend the relaxation RK methods to IMEX Runge–Kutta (IMEX RK) and the second–order multirate Runge–Kutta (MRK2) method [25]. Chemical kinetics [26], biochemical reactions [27], electrical circuits [28], and fluid mechanics [29] are all examples of stiff problems in many engineering and scientific applications. Partitioned Runge–Kutta (RK) methods define a class of integrators that use different time-stepping algorithms for different problem components. The aim of these methods is to avoid a monolithic algorithm when the problem at hand has components with different dynamical properties, which may require suitable

---

[1]The former mimics the integration by parts at a discrete level, and the latter unveil the mechanism underlying the skew-symmetric formulation. The split forms consist of both conservative and nonconservative forms of equations such that the aliasing errors caused by the volume integral terms become minimized.

[2]Classical explicit RK or linear multistep methods cannot preserve general quadratic invariants [18].

treatment for computational efficiency. Two of the most popular partitioned RK methods are implicit-explicit (IMEX) [30] and multirate [25].

IMEX schemes are widely used in multiscale problems including atmospheric [31, 32], ocean [33], sea-ice [34], shallow-water [29], and wind turbine models [35] and in plasma simulations [36]. By treating the fastest waves implicitly, IMEX methods overcome the stringent time step size of explicit methods and simplify the fully implicit system solves by using an explicit integrator for the nonstiff components. IMEX methods can also handle geometric-induced stiffness arising from mesh refinement by treating the fine-grid solution implicitly [37]. Similarly, multirate time integrators are a good candidate to tackle the stiffness issues. In multirate methods, an original problem is split into several subproblems, allowing different time step sizes on each subproblem. [3] Multirate methods are used in various applications such as atmospheric [38, 39] and air pollution models [40], the Burgers equation [25], Euler equations [41], and compressible Navier–Stokes equations [42].

Our proposed approaches not only alleviate the stiffness in a system but also provide entropy-preserving and entropy-stability properties at a fully discrete level. While the relaxation method is a straightforward step correction procedure, users will benefit from having a formula for partitioned Runge–Kutta methods. The presented methods could be a viable option to improve the robustness of stiff simulations. In particular, our contributions in this paper are as follows.

1. We derive the entropy-conserving/stable conditions for relaxation IMEX methods and provide an explicit relaxation expression for a class of IMEX methods.
2. We provide a similar result as above for partitioned multirate Runge–Kutta methods.
3. We demonstrate entropy stability and inner-product-based conservation on several numerical examples that employ IMEX methods for problems with stiff components and explicit multirate for problems with variable dynamical scales.

This paper is organized as follows. In Section 1.2 we describe the model problems and the one-dimensional entropy-conserving/stable discontinuous Galerkin spectral element method [8]. In Section 2 we introduce the entropy-conserving/stable IMEX and MRK2 methods and provide a novel analysis for the relaxation parameters of the IMEX-RK and MRK2 methods. In Section 3 we demonstrate the total mass conservation and the entropy conservation/stability of the proposed methods through numerical examples. Specifically, for the Burgers equation, we compare the relaxation approach and the incremental direction technique with and without a limiter in the vicinity of a shock. In Section 4 we present our conclusions.

---

[3] In IMEX methods, the same time step size is used for both sitff and nonstiff parts.

1.1. Problem Statement

Underresolved solutions cause aliasing errors, which can trigger numerical instability. This often happens when sharp gradient solutions are developed with insufficient spatial and temporal resolutions. One idea to maintain stability is to conserve or bound a quantity called entropy at a discrete level, which is a convex functional of the solution. Moreover, some applications require quadratic invariants preservation. This is not possible by directly using methods with explicit partitions. Relaxation methods have been proposed for monolithic, that is, single-partitioned (explicit), methods to overcome this limitation. This study extends the relaxation concept to two different classes of partitioned Runge–Kutta methods.

1.2. Model Problems and Spatial Discretization Methods

We introduce notation and model problems, along with a choice for the spatial discretization, making the presentation of the new time-stepping algorithms easier to follow.

1.2.1. Ordinary Differential Equation: Conserved Exponential Entropy

We consider the ordinary differential equation (ODE) example introduced in [24]:

$$\frac{d}{dt}\begin{pmatrix} q_1 \\ q_2 \end{pmatrix} = \begin{pmatrix} -\exp(q_2) \\ \exp(q_1) \end{pmatrix}. \tag{1}$$

This system preserves the exponential entropy of form

$$\eta(q) = \exp(q_1) + \exp(q_2).$$

1.2.2. Ordinary Differential Equation: Nonlinear Pendulum

We also consider the nonlinear pendulum described by the first-order ODE system

$$\frac{d}{dt}\begin{pmatrix} q_1 \\ q_2 \end{pmatrix} = \begin{pmatrix} -\sin(q_2) \\ q_1 \end{pmatrix}, \tag{2}$$

with initial condition $q = (1.5, 0)^T$ and entropy function $\eta(q) = 0.5q_1^2 - \cos(q_2)$.

1.2.3. Partial Differential Equation: The Burgers Equation

We consider the inviscid Burgers equation on the time and space interval $(t, x) \in [0, T] \times \Omega$:

$$\frac{\partial q}{\partial t} + \frac{1}{2}\frac{\partial q^2}{\partial x} = 0 \text{ in } [0, T] \times \Omega, \tag{3}$$

where q is a scalar quantity and $\Omega \subset \mathbb{R}$ is the one-dimensional domain. When considering implicit-explicit methods, we will split the spatial operator in two by defining a linearized flux F_L of $F := \frac{1}{2}q^2$ by

$$F_L := \tilde{q}q,$$

4

which will be treated implicitly, and the remaining nonlinear flux $\mathcal{F}_{\mathcal{N}}$

$$F_{\mathcal{N}} := \frac{q^2}{2} - \tilde{q}q \,,$$

with a reference state $\tilde{q}$ (for example, $\tilde{q} = q_n$: the numerical solution at t_n), which will be treated explicitly. We can now write (3) as the partitioned problem

$$\frac{\partial q}{\partial t} + \frac{\partial}{\partial x} \underbrace{(\tilde{q}q)}_{F_L} + \frac{\partial}{\partial x} \underbrace{\left(\frac{q^2}{2} - \tilde{q}q \right)}_{F_{\mathcal{N}}} = 0 \text{ in } \Omega \,. \tag{4}$$

1.2.4. Discontinuous Galerkin Spatial Discretization

We denote by $\Omega_h := \cup_{\ell=1}^{N_E} K_\ell$ the mesh containing a finite collection of non-overlapping elements, K_ℓ, that partition Ω, where N_E is the total number of elements. Let $\partial \Omega_h := \{ \partial K : K \in \Omega_h \}$ be the collection of the boundaries of all elements. For two neighboring elements K^+ and K^- that share an interior interface $\epsilon = K^+ \cap K^-$, we denote by $q^\pm$ the trace of the solutions on ϵ from $K^\pm$. We define $\mathbf{n}^-$ as the unit outward normal vector on the boundary ∂K^- of element K^- and $\mathbf{n}^+ = -\mathbf{n}^-$ as the unit outward normal of a neighboring element K^+. On the interior interfaces ϵ, we define the mean/average operator $\{\!\{v\}\!\}$, where v is a scalar quantity, by $\{\!\{v\}\!\} := \frac{1}{2} (v^- + v^+)$, and the jump operator $[\![v]\!] := v^+ \mathbf{n}^+ + v^- \mathbf{n}^-$.

Let $\mathcal{P}^N (D)$ denote the space of polynomials of degree at most N on a domain D. Next, we introduce the following discontinuous piecewise polynomial space as

$$V_h (\Omega_h) := \left\{ v \in L^2 (\Omega_h) : v|_K \in \mathcal{P}^N (K), \forall K \in \Omega_h \right\},$$

and similar spaces $V_h (K)$ by replacing Ω_h with K. We define $(\cdot, \cdot)_K$ as the L^2-inner product on an element K, and $\langle \cdot, \cdot \rangle_{\partial K}$ as the L^2-inner product on the element boundary ∂K. We also define the inner products as $(\cdot, \cdot)_{\Omega_h} := \sum_{K \in \Omega_h} (\cdot, \cdot)_K$ and $\langle \cdot, \cdot \rangle_{\partial \Omega_h} := \sum_{\partial K \in \partial \Omega_h} \langle \cdot, \cdot \rangle_{\partial K}$. We define associated norms as $\| \cdot \| := \| \cdot \|_{\Omega_h} := \left(\sum_{K \in \Omega_h} \| \cdot \|_K^2 \right)^{\frac{1}{2}}$, where $\| \cdot \|_K = (\cdot, \cdot)_K^{\frac{1}{2}}$.

The entropy-conserving/stable DG skew-symmetric formulation [8] of (3) is as follows: Seek $q_h \in V_h (\Omega_h)$ such that

$$\left(\frac{\partial q_h}{\partial t}, v \right)_{\Omega_h} := \langle \mathcal{R}(q_h), v \rangle \,, \tag{5}$$

where

$$\langle \mathcal{R}(q_h), v \rangle := \frac{2}{3} \left(\mathbb{I}^N \left(\frac{q_h^2}{2} \right), \frac{\partial v}{\partial x} \right)_{\Omega_h}$$

$$- \frac{1}{6} \left(\left(\mathbb{I}^N \left(q_h \frac{\partial q_h}{\partial x} \right), v \right)_{\Omega_h} - \left(q_h, \frac{\partial \mathbb{I}^N (q_h v)}{\partial x} \right)_{\Omega_h} \right) - \left\langle \mathbf{n} \frac{\widehat{q_h^2}}{2}, v \right\rangle_{\partial \Omega_h}$$

for all $v \in V_h(\Omega_h)$. Here, q_h is a polynomial approximation to q on each element K; that is, for $x \in K$, $q \approx q_h := \sum_{j=0}^{N} q_j(t)\ell_j(x)$ with nodal values of $u_j = u(x_j)$ and Lagrange basis function $\ell_j = \Pi_{k=0,k\neq j}^{N}\left(\frac{x-x_j}{x_k-x_j}\right)$ satisfying $\ell_j(x_i) = \delta_{ij}$ (for $j = 0, \cdots, N$); $\mathbb{I}^N()$ is the interpolation operator such that $\mathbb{I}^N(f) := \sum_{j=0}^{N} f(x_j)\ell_j(x)$; and $\widehat{f} = \widehat{\frac{q_h^2}{2}}$ is a numerical flux.

For the semi-discrete entropy-conserving formulation, we take the entropy-conserving flux,

$$\widehat{f}_{EC} := \frac{1}{6}\left((q_h^+)^2 + (q_h^-)^2 + q_h^- q_h^+\right);$$

and for the semi-discrete entropy-stable formulation, we use the Lax–Friedrichs flux,

$$\widehat{f}_{ES} := \left\{\!\!\left\{\frac{q_h^2}{2}\right\}\!\!\right\} + \frac{\tau}{2}[\![q_h]\!]$$

with $\tau := \max(|q_h^+|, |q_h^-|)$. The Lax–Friedrichs flux with the skew-symmetric formulation yields the energy-stable DG method [8].

The split form of the energy-conserving/stable DG weak formulation of (4) is as follows: seek $q_h \in V_h(\Omega_h)$ such that

$$\left(\frac{\partial q_h}{\partial t}, v\right)_{\Omega_h} := \langle Lq_h, v\rangle + \langle \mathcal{N}(q_h), v\rangle, \tag{6}$$

where

$$\langle Lq_h, v\rangle := -\frac{1}{2}\left(\mathbb{I}^N\left(\frac{\partial \tilde{q}_h q_h}{\partial x}\right), v\right)_{\Omega_h} + \frac{1}{2}\left(\mathbb{I}^N(\tilde{q}_h q_h), \frac{\partial v}{\partial x}\right)_{\Omega_h}$$
$$- \left\langle \mathbf{n}\left(\widehat{\tilde{q}_h q_h} - \frac{1}{2}\tilde{q}_h q_h\right), v\right\rangle_{\partial\Omega_h},$$
$$\langle \mathcal{N}(q_h), v\rangle := \langle \mathcal{R}(q_h), v\rangle - \langle Lq_h, v\rangle,$$

for all $v \in V_h(\Omega_h)$. We take $\widehat{\tilde{q}_h q_h} := \{\!\!\{\tilde{q}_h q_h\}\!\!\}$ for the entropy-conserving flux and $\widehat{\tilde{q}_h q_h} := \{\!\!\{\tilde{q}_h q_h\}\!\!\} + \frac{1}{2}\max(|\tilde{q}_h^\pm|)[\![q_h]\!]$ for the Lax–Friedrichs flux. The reference state $\tilde{q}_h$ is taken as the elementwise mean value of q_h at t_n, so that $\tilde{q}_h$ becomes a constant on each element.

1.2.5. Flux Limiters

Entropy-conserving/stable schemes are provably stable, but it is still not enough to eliminate high-frequency oscillations near a shock region. To control the Gibbs phenomenon, we employ the limiter proposed by [13]. The idea is to construct a linear function based on the two modified left and right values, $\check{q}^l$ and $\check{q}^r$ for each element,

$$\check{q}^l = \overline{q_h}_K - m\left(\overline{q_h}_K - q^l, \overline{q_h}_{K+1} - \overline{q_h}_K, \overline{q_h}_K - \overline{q_h}_{K-1}\right), \tag{7a}$$

$$\check{q}^r = \overline{q_h}_K + m\left(q^r - \overline{q_h}_K, \overline{q_h}_{K+1} - \overline{q_h}_K, \overline{q_h}_K - \overline{q_h}_{K-1}\right), \tag{7b}$$

$$\check{q} = \overline{q_h}_K + (q_K - \overline{q_h})\left(\frac{\check{q}^l + \check{q}^r - 2\overline{q_h}_K}{q^l + q^r - 2\overline{q_h}_K}\right), \tag{7c}$$

where $q^l := q_h(x_0)$ and $q^r := q_h(x_N)$ are the leftmost and the rightmost values on the Kth element, respectively; $\overline{q_h}_K$ is the mean value on the Kth element; and m is the minmod function defined by

$$
m(a, b, c) = \begin{cases} s \min(|a|, |b|, |c|), & \text{if } s = \text{ sgn}(a) = \text{ sgn}(b) = \text{ sgn}(c) \\ 0, & \text{otherwise} \end{cases} \,.
$$

Once a solution is integrated by one time step, we apply the limiter to the updated solution as a postprocessing task.

2. Entropy-Stable Time-Splitting Methods

In this section we propose entropy-conserving/stable IMEX and multirate methods by using relaxation methods.

Given a scalar hyperbolic equation,

$$
\frac{\partial q}{\partial t} + \frac{\partial F}{\partial x} = 0, \tag{8}
$$

where $x \in \Omega$ with Ω convex, we define a convex function $\eta : \Omega \to \mathbb{R}$ called an entropy function if there exists the entropy flux $\mathcal{F}$ satisfying $\frac{\partial \eta}{\partial q} \frac{\partial F}{\partial x} = \frac{\partial \mathcal{F}}{\partial x}$ and $\mathcal{F} = \varphi F - \psi$. Here, $\varphi := \frac{\partial \eta}{\partial q}$ and ψ are the entropy variable and potential flux, respectively. We multiply the entropy variable to (8) and integrate it over the domain, arriving at the tendency of the entropy function,

$$
\left(\frac{\partial \eta}{\partial t}, 1 \right)_{\Omega_h} = - \langle \mathbf{n} \mathcal{F}, 1 \rangle_{\partial \Omega_h}.
$$

[4] For a dissipative system, the entropy tendency should decrease:

$$
\left(\frac{\partial \eta}{\partial t}, 1 \right)_{\Omega_h} \leq - \langle \mathbf{n} \mathcal{F}, 1 \rangle_{\partial \Omega_h}. \tag{9}
$$

With periodic or compactly supported boundary conditions, the term on the right-hand side vanishes; hence, the semi-discrete entropy stability is guaranteed. For a fully discretized system, we expect

$$
(\eta(q_{h,n+1}), 1)_{\Omega_h} \leq (\eta(q_{h,n}), 1)_{\Omega_h}
$$

at a discrete level for a dissipative system; however, in practice the entropy condition is not guaranteed for all times. Here, $q_{h,n}$ and $q_{h,n+1}$ are approximations to q at $t = t_n$ and $t = t_{n+1}$, respectively. We will not include the subscript Ω_h in the inner product and h in q unless it is required explicitly.

---

[4]Here, we have used a chain rule, $\frac{\partial \eta}{\partial t} = \frac{\partial \eta}{\partial q} \frac{\partial q}{\partial t} = \varphi \frac{\partial q}{\partial t}$.

Remark 1. *For the Burgers equation, with the entropy function $\eta = \frac{q^2}{2}$ and entropy flux $\mathcal{F} = \frac{q^3}{3}$ [43], the semi-discrete form in* (9) *yields*

$$\frac{1}{2}\frac{d}{dt}\|q\|^2 \leq \langle q, \mathcal{R}(q)\rangle,$$

where $\mathcal{R}(q)$ is in (5). *The entropy stability implies L^2 stability.*

2.1. Relaxation Runge–Kutta Method

The standard explicit RK methods are

$$Q_i = q_n + \triangle t \sum_{j=1}^{i-1} a_{ij} R_j, \quad i = 1, 2, \cdots, s,$$

$$q_{n+1} = q_n + \triangle t \sum_{i=1}^{s} b_i R_i,$$

where $R_i := R(Q_i)$ and a_{ij} and b_i are scalar coefficients for s-stage RK methods. The basic idea of the relaxation Runge–Kutta method [18, 24] is to adjust the step completion with the relaxation parameter γ, effectively taking a modified step size such that the entropy stability is ensured. The time-adjusted solution at $t_{n+\gamma}(= t_n + \gamma\triangle t)$ is

$$q(t_n + \gamma\triangle t) \approx q_{n+\gamma} = q_n + \gamma\triangle t \sum_{i=1}^{s} (b_i R_i) = \gamma q_{n+1} + (1 - \gamma)q_n.$$

[5] The change in the entropy from t_n to $t_{n+\gamma}$ can be expressed as

$$\eta(q_{n+\gamma}) - \eta(q_n) = \underbrace{\eta(q_{n+\gamma}) - \eta(q_n) - \gamma\triangle t \sum_{i=1}^{s} b_i (R_i, \varphi_i)}_{:=\theta(\gamma)}$$
$$+ \gamma\triangle t \sum_{i=1}^{s} b_i (R_i, \varphi_i)$$

with $\varphi_i := \varphi(Q_i)$. The last term on the right-hand side is smaller than or equal to zero, provided by $\gamma > 0$ and $b_i \geq 0$. With a root γ of $\theta(\gamma) = 0$, the total entropy is bounded, $\eta(q_{n+\gamma}) \leq \eta(q_n)$. Here the nonlinear scalar equation $\theta(\gamma) = 0$ can be solved, for example, by Brent's method, the Levenberg–Marquard algorithm, or Newton's method [24, 22].

Remark 2. *The scheme using the $q(t_n + \triangle t) \approx q_{n+\gamma}$ approximation is referred to as an incremental direction technique (IDT) method [44]. The work in [18, Theorem 2.7] shows that the IDT method is one order less accurate than the relaxation approach.*

---

[5]This is simply a weighted sum of the current and the next step solutions.

2.2. Relaxation IMEX Methods

Consider a semi-discretized system,

$$\frac{\partial q}{\partial t} = R(q) = f(q) + g(q).$$

Recall s-stage IMEX-RK methods [30, 45, 46, 47],

$$Q_{n,i} = q_n + \triangle t \sum_{j=1}^{i-1} a_{ij} f_j + \triangle t \sum_{j=1}^{i} \tilde{a}_{ij} g_j, \quad i = 1, \ldots, s, \tag{10a}$$

$$q_{n+1} = q_n + \triangle t \sum_{i=1}^{s} b_i f_i + \triangle t \sum_{i=1}^{s} \tilde{b}_i g_i, \tag{10b}$$

where $f_i = f(t_n + c_i \triangle t, Q_{n,i})$, $g_i = g(t_n + \tilde{c}_i \triangle t, Q_{n,i})$, $q_n = q(t_n)$; $Q_{n,i}$ is the ith intermediate state; and $\triangle t$ is the time step size. The scalar coefficients a_{ij}, $\tilde{a}_{ij}$, b_i, $\tilde{b}_i$, c_i, and $\tilde{c}_i$ determine all the properties of a given IMEX-RK scheme. For each stage, the intermediate state $Q_{n,i}$ is obtained in general by a nonlinear solve,

$$Q_{n,i} - \tilde{a}_{ii} \triangle t g_j = q_n + \triangle t \sum_{j=1}^{i-1} (a_{ij} f_j + \tilde{a}_{ij} g_j).$$

Remark 3. *A practical way to avoid the nonlinear solve is to linearize the flux. To that end, we define a linear operator $L(\tilde{q}) := \frac{\partial R}{\partial q}\big|_{\tilde{q}}$ and choose $f(q) := R(q) - Lq$ and $g(q) := Lq$, where $\tilde{q}$ can be q_n or $Q_{n,i}$, $i = 1, \ldots, s$. Then at each stage the intermediate state $Q_{n,i}$ requires only a linear solve:*

$$Q_{n,i} - \tilde{a}_{ii} \triangle t L_i Q_{n,i} = q_n + \triangle t \sum_{j=1}^{i-1} (a_{ij} N_j + \tilde{a}_{ij} L_j Q_{n,j}), \tag{11}$$

where $R_i = R(t_n + c_i \triangle t, Q_{n,i})$, $L_i = L(t_n + c_i \triangle t, \tilde{q}) Q_{n,i}$, and $N_i = R_i - L_i$.

The relaxation IMEX-RK methods adjust the final time step size by

$$q(t_n + \gamma \triangle t) \approx q_{n+\gamma} = q_n + \gamma \triangle t \sum_{i=1}^{s} \left(b_i f_i + \tilde{b}_i g_i \right) = \gamma q_{n+1} + (1 - \gamma) q_n. \tag{12}$$

Now, the change in the entropy from t_n to $t_{n+\gamma}$ becomes

$$\eta(q_{n+\gamma}) - \eta(q_n) = \underbrace{\eta(q_{n+\gamma}) - \eta(q_n) - \gamma \triangle t \sum_{i=1}^{s} \left(b_i f_i + \tilde{b}_i g_i, \varphi_i \right)}_{:=\theta(\gamma)}$$
$$+ \gamma \triangle t \sum_{i=1}^{s} \left(b_i f_i + \tilde{b}_i g_i, \varphi_i \right). \tag{13}$$

9

Proposition 2.1. *The relaxation IMEX-RK methods in* (10a), (10b), *and* (12) *are entropy-conserving/stable with an entropy-conserving/stable spatial discretization of* $f(q)$ *and* $g(q)$ *and the relaxation parameter such that*

$$\eta(q_{n+\gamma}) - \eta(q_n) - \gamma \triangle t \sum_{i=1}^{s} \left(b_i f_i + \tilde{b}_i g_i, \varphi_i \right) = 0. \tag{14}$$

In particular, for energy entropy $\eta(q) = \frac{1}{2}\|q\|^2$, *the relaxation parameter is explicitly determined by*

$$\gamma = 2\|q_{n+1} - q_n\|^{-2} \triangle t \sum_{i=1}^{s} \left(b_i f_i + \tilde{b}_i g_i, Q_{n,i} - q_n \right).$$

Proof. By solving (14) for γ, the first, second, and third terms in (13) vanish. With an entropy-conserving/stable spatial discretization of f and g, the last term in (13) becomes nonpositive, that is, $(f_i, \varphi_i) \leq 0$ and $(g_i, \varphi_i) \leq 0$ for $i = 1, \cdots, s$, and hence $\eta(q_{n+\gamma}) \leq \eta(q_n)$.

By substituting η with the inner-product norm $\frac{1}{2}\|q\|^2$ and by using (10b), (14) can be written as

$$\|q_{n+\gamma}\|^2 - \|q_n\|^2 - 2\gamma \triangle t \sum_{i=1}^{s} \left(b_i f_i + \tilde{b}_i g_i, Q_{n,i} \right)$$

$$= \|\gamma (q_{n+1} - q_n) + q_n\|^2 - \|q_n\|^2 - 2\gamma \triangle t \sum_{i=1}^{s} \left(b_i f_i + \tilde{b}_i g_i, Q_{n,i} \right)$$

$$= \gamma^2 \|q_{n+1} - q_n\|^2 + 2\gamma (q_{n+1} - q_n, q_n) - 2\gamma \triangle t \sum_{i=1}^{s} \left(b_i f_i + \tilde{b}_i g_i, Q_{n,i} \right)$$

$$= \gamma^2 \|q_{n+1} - q_n\|^2 - 2\gamma \triangle t \sum_{i=1}^{s} \left(b_i f_i + \tilde{b}_i g_i, Q_{n,i} - q_n \right) = 0.$$

Rearranging a nonzero γ leads to the desired result. $\qquad\qquad\square$

Corollary 2.1.1. *The relaxation IMEX-RK methods with* $b_i = \tilde{b}_i$ *in* (10a), (10b), *and* (12) *are entropy conserving/stable with an entropy-conserving/stable spatial discretization* $R(q) = f(q) + g(q)$ *and the relaxation parameter*

$$\eta(q_{n+\gamma}) - \eta(q_n) - \gamma \triangle t \sum_{i=1}^{s} b_i (R_i, \varphi_i) = 0. \tag{15}$$

In particular, for the energy entropy $\eta(q) = \frac{1}{2}\|q\|^2$ *and nonstationary solution, the relaxation parameter is explicitly determined by*

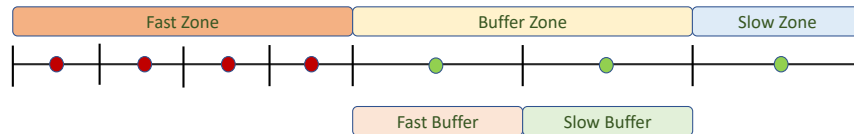$$\gamma = 2\|q_{n+1} - q_n\|^{-2} \triangle t \sum_{i=1}^{s} b_i (R_i, Q_{n,i} - q_n).$$

Figure 1: Illustration of MRK2 with a two-level decomposition: a domain is decomposed into fine (●) and coarse regions (●). Depending on the grid size and the location, the fast, the buffer, and the slow zones are identified. The fine region is considered the fast zone. The coarse regions are composed of the buffer zone and the slow zone. The buffer next to the fast zone is the fast buffer, while the buffer next to the slow zone is the slow buffer.

2.3. Relaxation Multirate Runge–Kutta Method

We apply the relaxation approach to the second-order multirate Runge–Kutta method [25]. The MRK2 method is based on a partitioned Runge–Kutta method where the second-order strong-stability-preserving Runge–Kutta [48] serves as the base method; further details are given in [25].

Multirate methods can be applied in different contexts. To simplify the exposition and without the loss of generality, however, we focus here on geometric-induced stiffness. We consider that some parts of a domain are spatially refined with a fixed 2:1 balancing ratio; that is, the ratio of an element size to its adjacent element size is at most 2. In the following, we first consider a two-level decomposition and then generalize the idea to an arbitrary-level domain decomposition.

2.3.1. Two-Level Decomposition

A domain is decomposed into two subdomains: coarse and fine regions with the ratio of a 2:1 grid size. Depending on the grid size and the location, the fast, the buffer, and the slow zones are identified as shown in Figure 1. The fine region is considered the fast zone. The coarse regions are composed of the buffer zone and the slow zone. The buffer next to the fast zone is the fast buffer, while the buffer next to the slow zone is the slow buffer.

Table 1 shows the Butcher tableau for MRK2 with a two-level decomposition. There are four global stages in all ($s = 4$). The solution on each element is updated depending on what region the element belongs to: the fast zone, the fast buffer, the slow buffer, and the slow zone. We assign zone number 1 for the fast zone, 2 for the fast buffer, 3 for the slow buffer, and 4 for the slow zone. The intermediate states and the next step solution for each zone number z are

$$Q_{n,i}^{\{z\}} = q_n^{\{z\}} + \triangle t \sum_{j=1}^{i-1} a_{ij}^{\{z\}} R_j^{\{z\}}, \quad i = 1, 2, \cdots, s, \tag{16a}$$

$$q_{n+1}^{\{z\}} = q_n^{\{z\}} + \triangle t \sum_{i=1}^{s} b_i^{\{z\}} R_i^{\{z\}} \tag{16b}$$

for $z = 1, \cdots, 4$.

Table 1: Butcher tableau for MRK2 with a two-level decomposition.

$$
\begin{array}{c|cccc}
0 & & & & \\
1/2 & 1/2 & & & \\
1/2 & 1/4 & 1/4 & & \\
1 & 1/4 & 1/4 & 1/2 & \\
\hline
 & 1/4 & 1/4 & 1/4 & 1/4
\end{array}
\qquad
\begin{array}{c|cccc}
0 & & & & \\
1 & 1 & & & \\
0 & 0 & 0 & & \\
1 & 0 & 0 & 1 & \\
\hline
 & 1/4 & 1/4 & 1/4 & 1/4
\end{array}
\qquad
\begin{array}{c|cccc}
0 & & & & \\
1 & 1 & & & \\
0 & 0 & 0 & & \\
1 & 1 & 0 & 0 & \\
\hline
 & 1/2 & 0 & 0 & 1/2
\end{array}
$$

(a) Fast zone/buffer   (b) Slow buffer   (c) Slow zone

The relaxation MRK2 for a two-level decomposition is

$$
q^{\{z\}}(t_n + \gamma \triangle t) \approx q_{n+\gamma}^{\{z\}} = q_n^{\{z\}} + \gamma \triangle t \sum_{i=1}^{s} b_i R_i^{\{z\}} = \gamma q_{n+1}^{\{z\}} + (1-\gamma) q_n^{\{z\}} \quad (17)
$$

for $z = 1, \cdots, 4$.

Proposition 2.2. *The relaxation MRK2 method for a two-level decomposition in* (16a), (16b), *and* (17) *are entropy conserving/stable with an entropy-conserving/stable spatial discretization R and the relaxation parameter satisfying*

$$
\eta(q_{n+\gamma}) - \eta(q_n) - \gamma \triangle t \sum_{z=1}^{4} \sum_{i=1}^{s} b_i^{\{z\}} \left(R_i^{\{z\}}, \varphi_{n,i}^{\{z\}} \right) = 0. \tag{18}
$$

For the quadratic invariant $\frac{1}{2}\|q\|^2$ and a dynamic solution ($q_{n+1}^{\{z\}} \neq q_n^{\{z\}}$), the relaxation parameter is explicitly determined:

$$
\gamma = 2 \left(\sum_{z=1}^{4} \|q_{n+1}^{\{z\}} - q_n^{\{z\}}\|^2 \right)^{-1} \left((\triangle t)^2 \sum_{z=1}^{4} \sum_{i=1}^{s} b_i^{\{z\}} \left(R_i^{\{z\}}, \frac{\left(Q_{n,i}^{\{z\}} - q_n^{\{z\}} \right)}{\triangle t} \right) \right).
$$

Proof. The change in the entropy from t_n to $t_{n+\gamma}$ becomes

$$
\eta(q_{n+\gamma}) - \eta(q_n) = \underbrace{\eta(q_{n+\gamma}) - \eta(q_n) - \gamma \triangle t \sum_{z=1}^{4} \sum_{i=1}^{s} b_i^{\{z\}} \left(R_i^{\{z\}}, \varphi_{n,i}^{\{z\}} \right)}_{:=\theta(\gamma)}
$$
$$
+ \gamma \triangle t \sum_{z=1}^{4} \sum_{i=1}^{s} b_i^{\{z\}} \left(R_i^{\{z\}}, \varphi_{n,i}^{\{z\}} \right). \quad (19)
$$

By solving (18) for γ, the first, second, and third terms in (19) vanish just as in the IMEX case. With an entropy-conserving/stable spatial discretization of R, the last term in (19) becomes again nonpositive.

By substituting η with the inner-product norm $\frac{1}{2}\|q\|^2$ and by using (16b), (18) becomes

$$
\|q_{n+\gamma}\|^2 - \|q_n\|^2 - 2\gamma\triangle t \sum_{z=1}^{4}\sum_{i=1}^{s} b_i^{\{z\}}\left(R_i^{\{z\}}, Q_{n,i}^{\{z\}}\right)
$$

$$
= \gamma^2\|q_{n+1} - q_n\|^2 + 2\gamma\sum_{z=1}^{4}\left(q_{n+1}^{\{z\}} - q_n^{\{z\}}, q_n^{\{z\}}\right) - 2\gamma\triangle t\sum_{z=1}^{4}\sum_{i=1}^{s} b_i^{\{z\}}\left(R_i^{\{z\}}, Q_{n,i}^{\{z\}}\right)
$$

$$
= \gamma^2\|q_{n+1} - q_n\|^2 - 2\gamma\triangle t\sum_{z=1}^{4}\sum_{i=1}^{s} b_i^{\{z\}}\left(R_i^{\{z\}}, Q_{n,i}^{\{z\}} - q_n^{\{z\}}\right) = 0.
$$

Rearranging the last equation yields an explicit form for γ. $\qquad\square$

At each stage, communication occurs between the fast zone and the fast buffer and between the fast buffer and the slow buffer. However, communication happens only at the first and the last stages between the slow buffer and the slow zone. After exchanging the interface data at the fourth stage, the right-hand side of the slow buffer at the second stage is evaluated. Based on this observation, we group the fast zone, the fast buffer, and the slow buffer by a level block that has four stages, which we call a cycle. We will use the level block notation for multilevel decomposition in the next section.

2.3.2. Beyond Two-Level Decomposition

We start by defining a level block. A level block (B) is formed by consecutive elements with the same multirate level (ℓ), each of which is assigned to a zone number (z). That means a level block (B) consists of a fast zone (fz), fast buffer (fb), and slow buffer (sb). [6] A level block (B) can have a neighbor level block $(\mathcal{N}(B))$ that has $\ell \pm 1$ multirate level. We let $L_{\max}$ be the maximum level and 0 be the minimum (root) level. We let $s_G := 2^{L_{\max}+1}$ be the total number of global stages and let $s^{\{0\}} = 2$ and $s^{\{\ell(B)\}} = 4$ (for $\ell = 1, 2, \cdots$) be the total number of local stages of a level block (B). We also let $m(B) := 2^{\{\ell(B)\}-1}$ be the number of substeps and $\triangle t^{\{\ell(B)\}} := \left(\frac{1}{2}\right)^{\ell(B)-1}\triangle t$ be the local time step size of a level block (B) so that $m(B)\triangle t^{\{\ell(B)\}} = \triangle t$ if $\ell(B) > 0$. When $\ell(B) = 0$, we take $m(B) = 1$. We assume that each fast buffer (fz) and slow buffer (sb) consist of one element.

The intermediate states and the next step solution of a level block (B) and

---

[6] We view the fast zone of level ℓ as the slow zone with respect to level $\ell + 1$. For instance, the level blocks with level 0 and level 1 in Figure 2 correspond to the fast zone, the buffer zone, and the slow zone in Figure 1.

a zone number (z) are written as

$$Q_{n+\frac{k}{m(B)},i}^{\{B,z\}} = q_{n+\frac{k}{m(B)}}^{\{B,z\}} + \triangle t^{\{\ell(B)\}} \sum_{j=1}^{i-1} a_{ij}^{\{z\}} R_{n+\frac{k}{m(B)},j}^{\{B,z\}}, \tag{20a}$$

$$q_{n+1}^{\{B,z\}} = q_n^{\{B,z\}} + \triangle t^{\{\ell(B)\}} \sum_{r=1}^{m(B)} \sum_{i=1}^{s^{\{\ell(B)\}}} b_i^{\{z\}} R_{n+\frac{r-1}{m(B)},i}^{\{B,z\}}, \tag{20b}$$

where

$$q_{n+\frac{k}{m(B)}}^{\{B,z\}} = q_n^{\{B,z\}} + \triangle t^{\{\ell(B)\}} \sum_{r=1}^{k} \sum_{i=1}^{s^{\{\ell(B)\}}} b_i^{\{z\}} R_{n+\frac{r-1}{m(B)},i}^{\{B,z\}},$$

for $k = 0, 1, \cdots, m(B) - 1$ and $i = 1, \cdots, s^{\{\ell(B)\}}$.

At the first global stage, all level blocks are activated, which means that the intermediate states of all the level blocks are updated and exchanged between adjacent active level blocks. At the second and the third global stages, the level blocks that have the maximum level $L_{\max}$ are activated. At the fourth global stage, the level blocks that have $L_{\max}$ and $L_{\max-1}$ levels are activated. This implies that after one cycle, these level blocks are synchronized. This process is repeated until all the level blocks are synchronized at the last global stage, s_G. We construct the activation table in Algorithm 1 to control the synchronization. That is, according to the activation table, certain level blocks are activated at a given global stage.

Algorithm 1 Activation Table for Level Blocks

Ensure: Given the maximum level ($L_{\max}$), construct the activation table ($actvTable$) of the size $s_G \times N_B$. Here, N_B is the total number of level blocks.

1: $actvTable[:,:] = 0$
2: **for** B in $\{1 : N_B\}$ **do**
3:      $nActv \leftarrow 2^{\ell(B)}$
4:      $d \leftarrow 2^{(L_{\max}+1-\ell(B))}$
5:      **for** $i = 1 : nActv$ **do**
6:          $actvTable[\,1 + d(i-1), B] \leftarrow 1$
7:          $actvTable[s_G - d(i-1), B] \leftarrow 1$
8:      **end for**
9: **end for**

We give an example with a three-level decomposition in Figure 2, where three level blocks (B_1, B_2, and B_3) have 0, 1, and 2 multirate levels, respectively. The maximum level is two, $L_{\max} = 2$; thus the total number of global stage becomes $s_G = 8$. B_1 and B_2 have one subcycle ($m(B_1) = m(B_2) = 1$), and B_3 has two subcycles ($m(B_3) = 2$). At every subcycle, a level block (B) needs to be synchronized with its neighbors ($\mathcal{N}(B)$). The B_3 level block communicates with
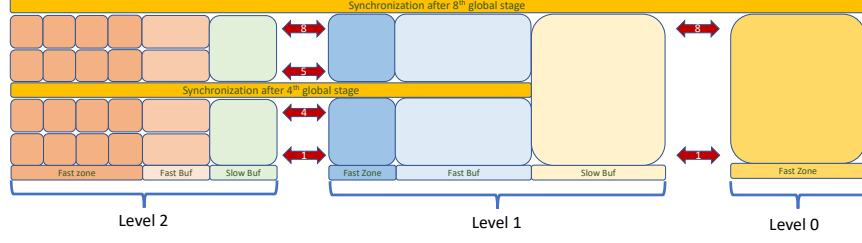
Figure 2: Illustration of MRK2 with a three-level decomposition: three level blocks (B_1, B_2, and B_3) have 0, 1, and 2 multirate levels, respectively. Each level block is composed of the fast zone, the fast buffer, and the slow buffer. The maximum level is two, $L_{\max} = 2$. The number of global stages (the depth of MRK2) is $8 (= 2^{L_{\max}+1})$, and the number of local stage of each level is 4 (except level 0). The B_3 level block communicates with B_2 level block at four stages (i.e., 1, 4, 5, and 8 global stages), whereas the B_2 level block exchanges interface data with the B_1 level block at two stages (i.e., 1 and 8 global stages).

the B_2 level block at four stages (i.e., 1, 4, 5, and 8 global stages), whereas the B_2 level block exchanges the interface data with the B_1 level block at two stages (i.e., 1 and 8 global stages).

The intermediate states and the next step solution corresponding to Figure 2 yield

$$Q_{n,i}^{\{B_1,z\}} = q_n^{\{B_1,z\}} + 2\triangle t \sum_{j=1}^{2} a_{ij}^{\{z\}} R_{n,j}^{\{B_1,z\}} \quad i = 1, 2,$$

$$Q_{n+\frac{0}{1},i}^{\{B_2,z\}} = q_n^{\{B_2,z\}} + \triangle t \sum_{j=1}^{4} a_{ij}^{\{z\}} R_{n,j}^{\{B_2,z\}} \quad i = 1, \cdots, 4,$$

$$Q_{n+\frac{0}{2},i}^{\{B_3,z\}} = q_n^{\{B_3,z\}} + \frac{\triangle t}{2} \sum_{j=1}^{4} a_{ij}^{\{z\}} R_{n,j}^{\{B_3,z\}} \quad i = 1, \cdots, 4,$$

$$Q_{n+\frac{1}{2},i}^{\{B_3,z\}} = q_{n+\frac{1}{2}}^{\{B_3,z\}} + \frac{\triangle t}{2} \sum_{j=1}^{4} a_{ij}^{\{z\}} R_{n+\frac{1}{2},j}^{\{B_3,z\}} \quad i = 1, \cdots, 4,$$

and

$$q_{n+1}^{\{B_1,z\}} = q_n^{\{B_1,z\}} + 2\triangle t \sum_{i=1}^{2} b_i^{\{z\}} R_{n,i}^{\{B_1,z\}},$$

$$q_{n+1}^{\{B_2,z\}} = q_n^{\{B_2,z\}} + \triangle t \sum_{i=1}^{4} b_i^{\{z\}} R_{n,i}^{\{B_2,z\}},$$

$$q_{n+1}^{\{B_3,z\}} = q_n^{\{B_3,z\}} + \frac{\triangle t}{2} \sum_{r=1}^{2} \sum_{i=1}^{4} b_i^{\{z\}} R_{n+\frac{r-1}{2},i}^{\{B_3,z\}},$$

15

where

$$q_{n+\frac{1}{2}}^{\{B_3,z\}} = q_n^{\{B_3,z\}} + \frac{\triangle t}{2} \sum_{i=1}^{4} b_i^{\{z\}} R_{n,i}^{\{B_3,z\}},$$

for $z = 1, 2, 3$.

The relaxation MRK2 for multilevel decomposition is

$$q_{n+\gamma}^{\{B,z\}} = q_n^{\{B,z\}} + \gamma \triangle t^{\{\ell(B)\}} \sum_{r=1}^{m(B)} \sum_{i=1}^{s^{\{\ell(B)\}}} b_i^{\{z\}} R_{n+\frac{r-1}{m(B)},i}^{\{B,z\}} \qquad (21)$$

for a level block B and a zone number z.

Proposition 2.3. *Let N_B be the number of level blocks. The relaxation MRK2 method for multilevel decomposition in* (20a), (20b), *and* (21) *are entropy conserving/stable with an entropy-conserving/stable spatial discretization $R(q)$ and the relaxation parameter*

$$\eta(q_{n+\gamma}) - \eta(q_n)$$
$$- \gamma \sum_{B=1}^{N_B} \triangle t^{\{\ell(B)\}} \sum_{z=1}^{3} \sum_{r=1}^{m(B)} \sum_{i=1}^{s^{\{\ell(B)\}}} b_i^{\{z\}} \left(R_{n+\frac{r-1}{m(B)},i}^{\{B,z\}}, \varphi_{n+\frac{r-1}{m(B)},i}^{\{B,z\}} \right) = 0. \quad (22)$$

For the quadratic invariant $\frac{1}{2}\|q\|^2$, the relaxation parameter is explicitly determined:

$$\gamma = 2 \left(\sum_{B=1}^{N_B} \sum_{z=1}^{3} \|q_{n+1}^{\{B,z\}} - q_n^{\{B,z\}}\|^2 \right)^{-1}$$
$$\left(\sum_{B=1}^{N_B} \triangle t^{\{\ell(B)\}} \sum_{z=1}^{3} \sum_{r=1}^{m(B)} \sum_{i=1}^{s^{\{\ell(B)\}}} b_i^{\{z\}} \left(R_{n+\frac{r-1}{m(B)},i}^{\{B,z\}}, Q_{n+\frac{r-1}{m(B)},i}^{\{B,z\}} - q_n^{\{B,z\}} \right) \right).$$

Proof. The change in the entropy from t_n to $t_{n+\gamma}$ becomes

$$\eta(q_{n+\gamma}) - \eta(q_n) =$$
$$\underbrace{\eta(q_{n+\gamma}) - \eta(q_n) - \gamma \sum_{B=1}^{N_B} \triangle t^{\{\ell(B)\}} \sum_{z=1}^{3} \sum_{r=1}^{m(B)} \sum_{i=1}^{s^{\{\ell(B)\}}} b_i^{\{z\}} \left(R_{n+\frac{r-1}{m(B)},i}^{\{B,z\}}, \varphi_{n+\frac{r-1}{m(B)},i}^{\{B,z\}} \right)}_{:=\theta(\gamma)}$$
$$+ \gamma \sum_{B=1}^{N_B} \triangle t^{\{\ell(B)\}} \sum_{z=1}^{3} \sum_{r=1}^{m(B)} \sum_{i=1}^{s^{\{\ell(B)\}}} b_i^{\{z\}} \left(R_{n+\frac{r-1}{m(B)},i}^{\{B,z\}}, \varphi_{n+\frac{r-1}{m(B)},i}^{\{B,z\}} \right). \quad (23)$$

By solving (22) for γ, the first, second, and third terms in (23) vanish as before. With an entropy-conserving/stable spatial discretization of R, the last term in (23) becomes nonpositive as expected.

16

By substituting η with the inner-product norm $\frac{1}{2}\|q\|^2$ and using (20b), (22) becomes

$$\|q_{n+\gamma}\|^2 - \|q_n\|^2 - 2\gamma \sum_{B=1}^{N_B} \triangle t^{\{\ell(B)\}} \sum_{z=1}^{3} \sum_{r=1}^{m(B)} \sum_{i=1}^{s^{\{\ell(B)\}}} b_i^{\{z\}} \left(R_{n+\frac{r-1}{m(B)},i}^{\{B,z\}}, Q_{n+\frac{r-1}{m(B)},i}^{\{B,z\}} \right)$$

$$= \gamma^2 \|q_{n+1} - q_n\|^2 + 2\gamma \sum_{B=1}^{N_B} \sum_{z=1}^{3} \left(q_{n+1}^{\{B,z\}} - q_n^{\{B,z\}}, q_n^{\{B,z\}} \right)$$

$$- 2\gamma \sum_{B=1}^{N_B} \triangle t^{\{\ell(B)\}} \sum_{z=1}^{3} \sum_{r=1}^{m(B)} \sum_{i=1}^{s^{\{\ell(B)\}}} b_i^{\{z\}} \left(R_{n+\frac{r-1}{m(B)},i}^{\{B,z\}}, Q_{n+\frac{r-1}{m(B)},i}^{\{B,z\}} \right)$$

$$= \gamma^2 \|q_{n+1} - q_n\|^2$$

$$- 2\gamma \sum_{B=1}^{N_B} \triangle t^{\{\ell(B)\}} \sum_{z=1}^{3} \sum_{r=1}^{m(B)} \sum_{i=1}^{s^{\{\ell(B)\}}} b_i^{\{z\}} \left(R_{n+\frac{r-1}{m(B)},i}^{\{B,z\}}, Q_{n+\frac{r-1}{m(B)},i}^{\{B,z\}} - q_n^{\{B,z\}} \right) = 0.$$

Rearranging the last equation yields the explicit γ. $\qquad\square$

For implementation, first we balance the multirate level of each element so that all the level blocks have a 2:1 local time step size ratio to their adjacent level blocks according to Algorithm 2. Next we construct the activation table in Algorithm 1. Then we compute the entropy-conserving/stable solutions according to (20).

3. Numerical Results

In this section we present several numerical experiments to demonstrate the entropy-conserving/stable properties of the proposed IMEX methods and the multirate methods. We compare standard methods, relaxation approaches, and incremental direction techniques for both IMEX and multirate methods. For IMEX methods, we use additive Runge–Kutta (ARK) methods [46], and call them Relaxation-ARK and IDT-ARK for their relaxation and incremental direction techniques, respectively. For multirate methods, we employ the second-order partitioned multirate Runge–Kutta (MRK2) methods [25], which we refer to as Relaxation-MRK2 and IDT-MRK2 for their relaxation and incremental direction techniques, respectively. We use the IMEX methods for handling scale-separable stiffness on a uniform mesh and the multirate method for dealing with geometric-induced stiffness on nonuniform meshes. We measure the L^2 error of q by $\|q - q_r\|$, where q_r is either an exact solution or a reference solution. The total entropy difference and the total mass difference are denoted by $|\eta(t) - \eta(0)|$ and $|\text{mass}(t) - \text{mass}(0)|$ at time t, where $\text{mass}(t) := (q, 1)$.

3.1. Entropy-Preserving IMEX for ODEs
Conserved Exponential Entropy

We take the initial condition of $q = (1, 0.5)^T$ for (1) and run the simulations for $t \in [0, 5]$ with $\triangle t = 0.1$. We plot the time series of the exponential

Algorithm 2 Balancing Multirate Level of Elements

Ensure: Let K be the total number of elements. Let $LE \in \mathbb{R}$ be the initial multirate levels of all elements. Let $BLE \in \mathbb{R}$ be the 2:1 balanced multirate levels of all elements. That is, a level jump between adjacent elements is at most one. Given LE, BLE is created. Let bs be the buffer size of two. We assume that $bs + 1$ left/right boundary elements have the same level, $LE_{(1:bs+1)} = \ell_{left}$ and $LE_{((K-bs):K)} = \ell_{right}$.

1: Compute level difference, $\delta LE_{(1:K-1)} = LE_{(2:K)} - LE_{(1:K-1)}$
2: $idx \leftarrow Find(\delta LE \neq 0)$
3: $cond = \mathbf{false}$; $BLE \leftarrow LE$
4: **while** $!cond$ **do**
5:    $cond = \mathbf{true}$
6:    **for** i in $\{1 : length(idx)\}$ **do**
7:       $iK_1 \leftarrow idx[i]$
8:       $iK_2 \leftarrow idx[i+1]$
9:       **if** $(\delta LE_{(iK_1)} == -1)$ and $(\delta LE_{(iK_2)} == -1)$ **then**
10:          **if** $(iK_2 - iK_1) < (bs + 1)$ **then**
11:             $cond = \mathbf{false}$
12:             $nc = (bs + 1) - (iK_2 - iK_1)$
13:             $BLE_{(iK_2+1:iK_2+nc)} = \max(BLE_{(iK_2+1:iK_2+nc)}, LE_{(iK_2)})$
14:          **end if**
15:       **else if** $(\delta LE_{(iK_1)} == -1)$ and $(\delta LE_{(iK_2)} == 1)$ **then**
16:          **if** $(iK_2 - iK_1) < (bs + 1)$ **then**
17:             $cond = \mathbf{false}$
18:             $BLE_{(iK_1+1:iK_2)} = \max(BLE_{(iK_2)}, LE_{(iK_1)})$
19:          **end if**
20:       **else if** $(\delta LE_{(iK_1)} == 1)$ and $(\delta LE_{(iK_2)} == 1)$ **then**
21:          $cond = \mathbf{false}$
22:          **if** $(iK_2 - iK_1) < (bs + 1)$ **then**
23:             $cond = \mathbf{false}$
24:             $nc = (bs + 1) - (iK_2 - iK_1)$
25:             $BLE_{(iK_1+1-nc:iK_1)} = \max(BLE_{(iK_1+1-nc:iK_1)}, LE_{(iK_2)})$
26:          **end if**
27:       **end if**
28:    **end for**
29:    Update level of elements, $LE \leftarrow BLE$
30:    Compute level difference, $\delta LE_{(1:K-1)} := LE_{(2:K)} - LE_{(1:K-1)} \in \mathbb{R}^{K-1}$
31:    $idx \leftarrow Find(\delta LE \neq 0)$
32: **end while**

---

entropy in Figure 3. We observe that the total entropy differences for both the Relaxation-ARK and IDT-ARK are below $\mathcal{O}(10^{-13})$, whereas the standard ARK counterpart shows a difference of orders of magnitude, such as $\mathcal{O}(10^{-3})$, as expected.
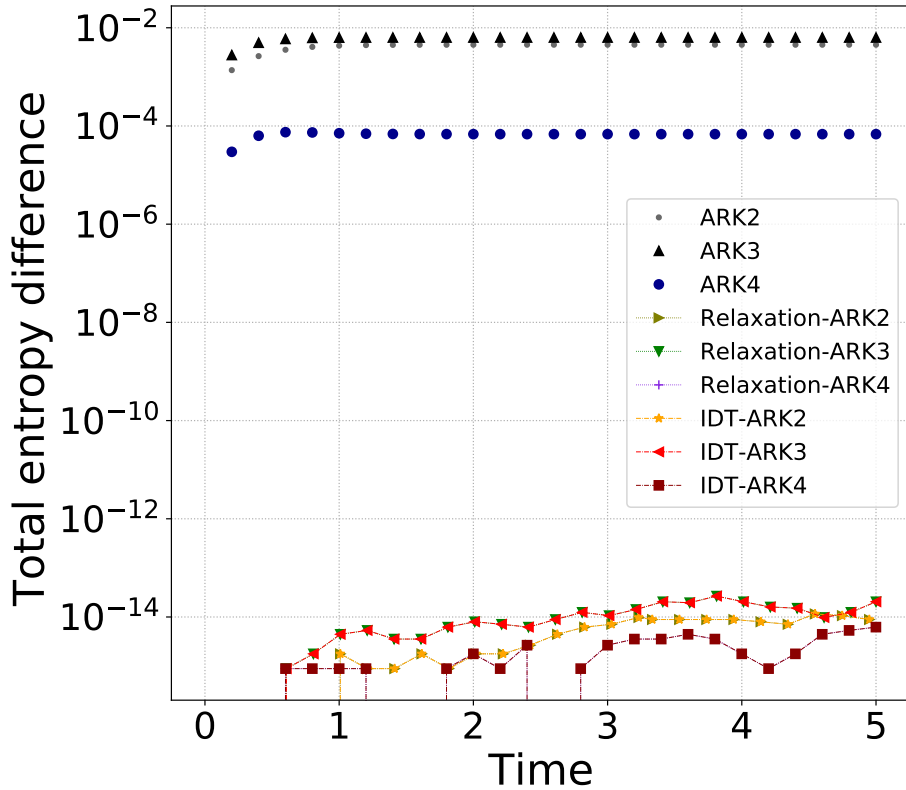
Figure 3: ODE: conserved exponential entropy. Total entropy differences for both the Relaxation-ARK and IDT-ARK are bounded within $\mathcal{O}(10^{-13})$, whereas the ARK counterpart shows a difference of orders of magnitude, $\mathcal{O}(10^{-3})$.

Nonlinear Pendulum

For (2) we examine the entropy behavior and the solution trajectory over time in Figure 4. We take $\triangle t = 0.9$ and run the simulations for $t \in [0, 1000]$. Both the Relaxation-ARK and IDT-ARK keep the pendulum in a track, but standard ARK methods cannot hold the pendulum in the path. The total entropy difference for both the Relaxation-ARK and IDT-ARK are bounded within $\mathcal{O}(10^{-13})$; however, as expected, standard ARK methods have $\mathcal{O}(1)$ entropy difference during the simulation.

3.2. Entropy-Stable IMEX for the Burgers Equation on a Uniform Mesh

We consider a Gaussian initial profile, which develops a shock as time passes for the Burgers equation. The initial condition is given as

$$q(t = 0) = \exp(-10x^2)$$

on $x \in [-1, 1]$. A periodic boundary condition is applied.

We first perform temporal convergence studies with entropy-conserving (EC) and entropy-stable (ES) fluxes for the ARK, Relaxation-ARK, and IDT-ARK methods. In particular, we use the IMEX methods based on the linearized flux in (6). We take the RK4 solution (with $\triangle t = 5 \times 10^{-6}$, $N = 3$, and $N_E = 100$) as the "ground truth" solution and measure the relative errors at $t = 0.2$ (before forming a shock) in Table 2 and Table 3.

(a) Trajectory
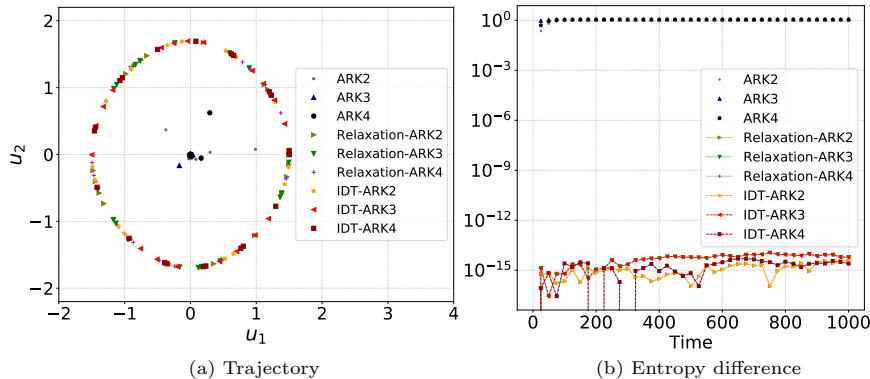
(b) Entropy difference

Figure 4: ODE: nonlinear pendulum. Both the Relaxation-ARK and IDT-ARK keep the pendulum in a track, but standard ARK methods cannot hold the pendulum on the exact path. The total entropy difference for both the Relaxation-ARK and IDT-ARK is bounded below $\mathcal{O}(10^{-13})$; however, standard ARK methods have $\mathcal{O}(1)$ entropy difference during the simulation.

In Table 2 we observe the second-order rate of convergence for both ARK2 and Relaxation-ARK2 with EC and ES fluxes. IDT-ARK2, however, shows the first-order rate of convergence. This is a consequence of the time discretization error of the IDT approach. Similarly, in Table 3, IDT-ARK3 shows a second-order rate of convergence, which is one degree less accurate than that of its ARK3 and Relaxation-ARK3 counterparts. As shown in both Table 2 and Table 3, the relative error of Relaxation-ARK methods is slightly lower than that of naive ARK methods.

To investigate the entropy-conserving properties of ARK methods, we conduct the numerical experiments for $t \in [0, 2]$ with a uniform mesh of $N = 3$ and $N_E = 800$. The time step size of RK2 is taken as $\triangle t_{RK} = 3.125 \times 10^{-5}$, whereas the time step sizes of ARK, Relaxation-ARK, and IDT-ARK have $5 \times \triangle t_{RK}$. [7] Figure 5 shows the time series of the total energy and its difference for the RK2, ARK2, Relaxation-ARK2, IDT-ARK2, ARK3, Relaxation-ARK3, and IDT-ARK3 methods. The second- and the third-order Relaxation-ARK and IDT-ARK methods conserve their total energies within $\mathcal{O}(10^{-13})$ differences, whereas ARK2 and ARK3 show a slightly decreasing trend of total energy. This is because IMEX methods act as a high-frequency filter by treating the fast-varying dynamics implicitly [29, 49]. As a result, energy-stable behavior is observed for the standard ARK methods. RK2, however, does not have any filter functionality, so its total energy shows an increasing trend.

We show snapshots at $t = 1$ in Figure 6. All numerical solutions suffer from high-frequency noise arising from the Gibbs phenomenon in the presence of a shock. However, the numerical solutions do not blow up thanks to the skew-symmetric formulation [8]. Compared with RK2, ARK2 dramatically eliminates the high-frequency oscillation. Relaxation-ARK2 and IDT-ARK2 also reduce the high-frequency oscillation but not as significantly as ARK2.

---

[7]RK2 with $2 \times \triangle t_{RK}$ leads to blow up its numerical solution.

(a) Total energy history (EC)
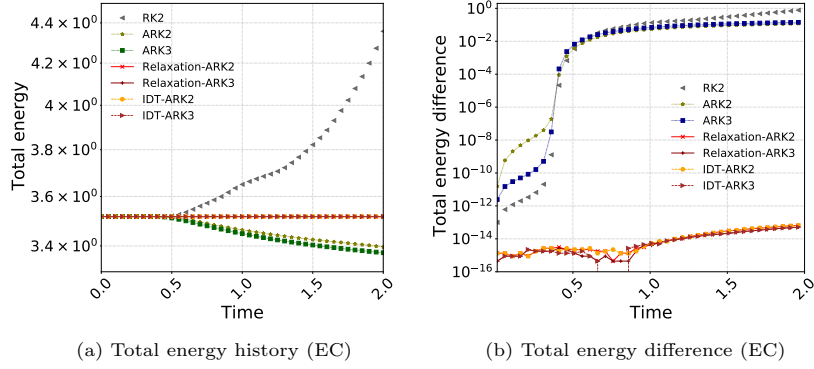
(b) Total energy difference (EC)

Figure 5: Histories of total entropy and its difference of Gaussian example for the Burgers equation with EC flux: the relaxation methods with EC flux conserve the total energy within $\mathcal{O}(10^{-13})$.
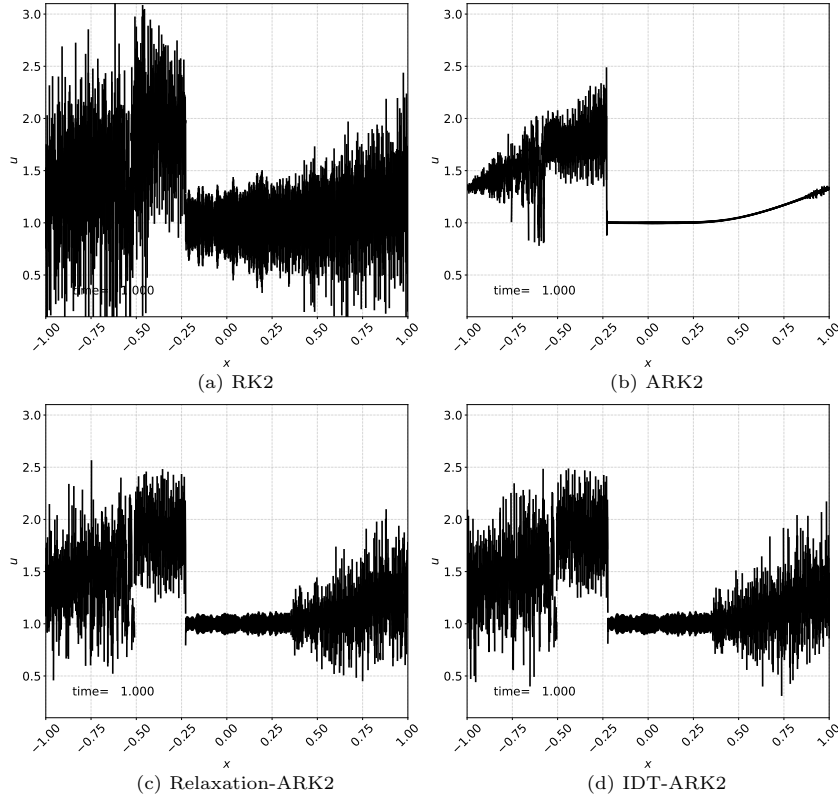

(a) RK2

(b) ARK2

(c) Relaxation-ARK2

(d) IDT-ARK2

Figure 6: Snapshots of Gaussian profile for the Burgers equation at $t = 1$: (a) RK2, (b) ARK2, (c) Relaxation-ARK2, and (d) IDT-ARK2. The time step size of RK2 is taken as $\triangle t_{RK} = 3.125 \times 10^{-5}$, whereas the time step sizes of ARK2, Relaxation-ARK2, and IDT-ARK2 have $5 \times \triangle t_{RK}$. The domain is discretized with a uniform mesh of $N = 3$ and $N_E = 800$.

21

Table 2: Gaussian example: temporal convergence study of ARK2 methods conducted on a uniform mesh of $N = 3$ and $K = 100$. Time step sizes are chosen as $\triangle t = 0.00125\,\{1, 1/2, 1/4, 1/8, 1/16\}$ with EC flux; and $\triangle t = 0.005\,\{1, 1/2, 1/4, 1/8, 1/16\}$ with ES flux. By taking the RK4 solution with $\triangle t = 5.0 \times 10^{-6}$ as the "ground truth" solution, we measure the relative errors of the ARK2, Relaxation-ARK2, and IDT-ARK2 methods at $t = 0.2$.

$flux$	dt	ARK2		Relaxation-ARK2		IDT-ARK2	
		Error	Order	Error	Order	Error	Order
EC	1.250e-03	1.60E-05	–	1.48E-05	–	1.30E-04	–
	6.250e-04	4.00E-06	2.00	3.71E-06	2.00	6.65E-05	0.97
	3.125e-04	1.00E-06	2.00	9.29E-07	2.00	3.37E-05	0.98
	1.563e-04	2.51E-07	2.00	2.32E-07	2.00	1.69E-05	0.99
	7.813e-05	6.27E-08	2.00	5.81E-08	2.00	8.49E-06	1.00
ES	5.000e-03	2.51E-04	–	2.32E-04	–	4.80E-04	–
	2.500e-03	6.36E-05	1.98	5.88E-05	1.98	2.50E-04	0.94
	1.250e-03	1.60E-05	1.99	1.48E-05	1.99	1.30E-04	0.94
	6.250e-04	4.00E-06	2.00	3.71E-06	2.00	6.65E-05	0.97
	3.125e-04	1.00E-06	2.00	9.29E-07	2.00	3.36E-05	0.98

Next we examine the entropy-stable properties of the ARK methods. We perform the simulations for $t \in [0, 2]$ with $N = 3$ and $N_E = 800$. The time step size of RK2 is taken as $\triangle t_{RK} = 2.5 \times 10^{-4}$, whereas the time step sizes of the other methods including the ARK2 method have $2.5 \times \triangle t_{RK}$. [8] Compared with EC flux, ES flux substantially eliminates numerical oscillations but still not enough to remove nonphysical oscillations near shocks. Thus, we additionally apply the limiter in (7) to a marched solution at every time step.

The snapshots at $t = 1$ are reported in Figure 7. All the methods with the limiter successfully eliminate the spurious oscillations near the shock front. The shock front, located near $x = -0.25$, is well captured for all methods with/without the limiter in general. However, the IDT-ARK2 method with the limiter shows the shock position error compared with other methods.

In Figure 8 the time histories of the total energy and its difference are reported for ARK2, Relaxation-ARK2, IDT-ARK2, ARK3, Relaxation-ARK3, and IDT-ARK3 with/without the limiter. (The RK2 result is also reported for comparison.) All the methods with ES flux show entropy-stable behaviors regardless of applying the limiter. This observation agrees with the work in [13, Theorem 3.8].

In Figure 9 we also plot the time series of the total mass (a linear invariant) for ARK2, Relaxation-ARK2, IDT-ARK2, ARK3, Relaxation-ARK3, and IDT-

---

[8]RK2 with $\triangle t_{RK} = 5 \times 10^{-4}$ leads to blowup of the numerical solution.

(a) RK2   (b) RK2 w/ limiter

(c) ARK2   (d) ARK2 w/ limiter

(e) Relaxation-ARK2   (f) Relaxation-ARK2 w/ limiter
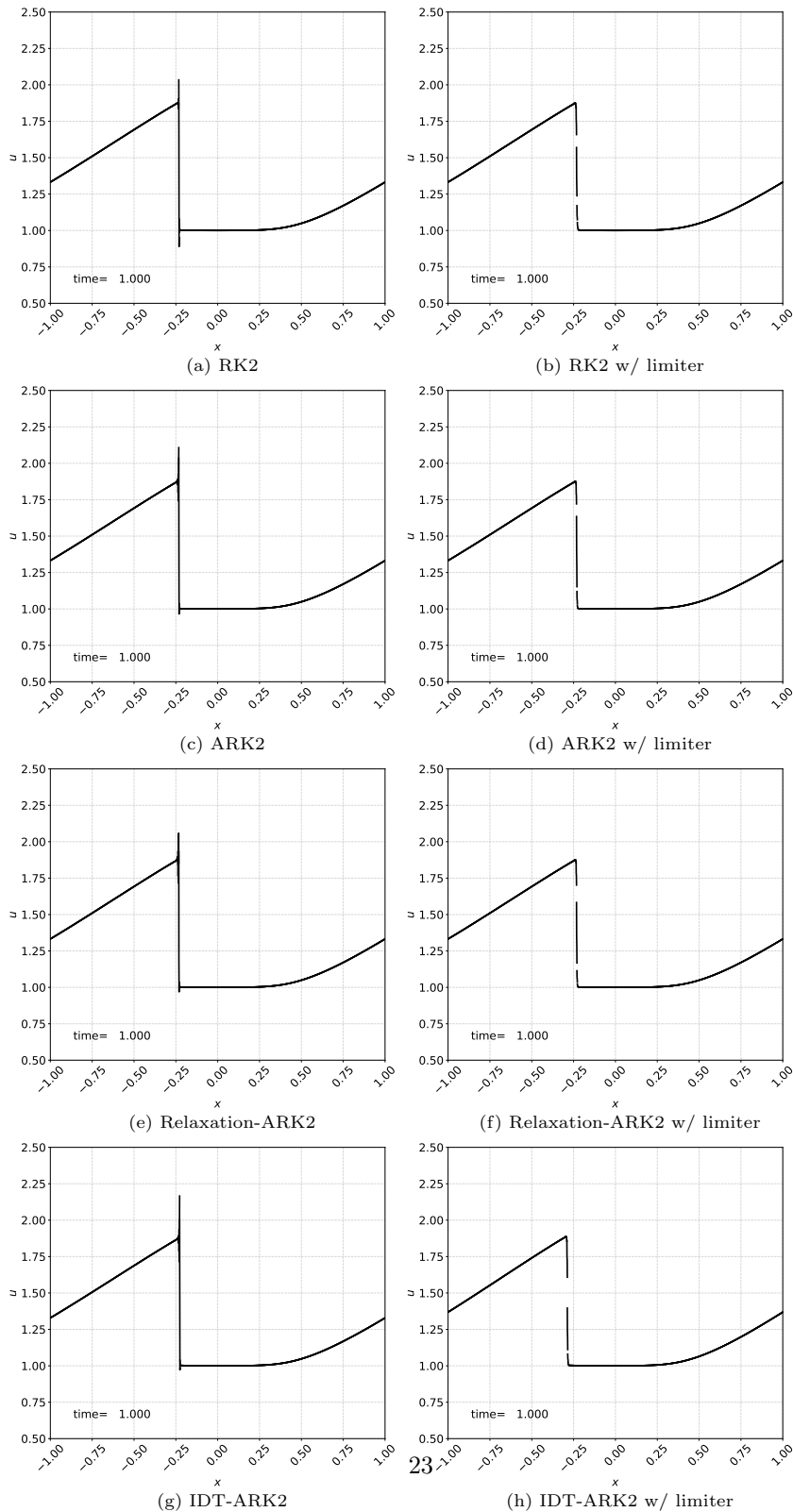
(g) IDT-ARK2   (h) IDT-ARK2 w/ limiter

Figure 7: Snapshots of Gaussian profile for the Burgers equation at $t = 1$ with entropy-stable (ES) flux for (a) RK2, (b) RK2 with the limiter, (c) ARK2, (d) ARK2 with the limiter, (e) Relaxation-ARK2, (f) Relaxation-ARK2 with the limiter, (g) IDT-ARK2, and (h) IDT-ARK2 with the limiter. The time step size of RK2 is taken as $\triangle t_{RK} = 2.5 \times 10^{-4}$, whereas the time step sizes of other methods have $2.5 \times \triangle t_{RK}$. The domain is discretized with a uniform mesh of $N = 3$ and $N_E = 800$.

Table 3: Same as 2, except the third-order accurate methods.

flux	$\triangle t$	ARK3		Relaxation-ARK3		IDT-ARK3	
		Error	Order	Error	Order	Error	Order
EC	1.250e-03	4.76E-07	–	4.53E-07	–	1.02E-05	–
	6.250e-04	6.03E-08	2.98	5.76E-08	2.98	2.54E-06	2.00
	3.125e-04	7.61E-09	2.99	7.29E-09	2.98	6.34E-07	2.00
	1.563e-04	9.58E-10	2.99	9.18E-10	2.99	1.58E-07	2.00
	7.813e-05	1.20E-10	2.99	1.15E-10	2.99	3.96E-08	2.00
ES	5.000e-03	2.76E-05	–	2.58E-05	–	1.65E-04	–
	2.500e-03	3.61E-06	2.93	3.41E-06	2.92	4.09E-05	2.01
	1.250e-03	4.59E-07	2.97	4.36E-07	2.97	1.02E-05	2.01
	6.250e-04	5.79E-08	2.99	5.51E-08	2.99	2.54E-06	2.00
	3.125e-04	7.26E-09	3.00	6.92E-09	2.99	6.34E-07	2.00

ARK3 with/without limiter, as well as RK2. As expected, all the methods preserve the total mass within $\mathcal{O}(10^{-14})$ difference.

3.3. Entropy-Stable Multirate Methods for the Burgers Equation on a Nonuniform Mesh

We consider MRK2 methods on a nonuniform mesh for handling geometric-induced stiffness. A one-dimensional domain is five times refined at the center of the domain with a 2:1 grid ratio so that the biggest element is 32 times larger than the smallest element, as shown in Figure 10a. In the MRK2 algorithm, based on the ratio of the element sizes, multirate levels are assigned to each element in Figure 10b, where the highest multirate level is five.

We first perform temporal convergence studies with the entropy-conserving and entropy-stable fluxes for MRK2, Relaxation-MRK2, and IDT-MRK2 methods without using the limiter. We take the RK4 solution (with the fixed step size of $\triangle t = 5 \times 10^{-6}$, $N = 3$, and $N_E = 196$) as the "ground truth" solution and measure the relative errors at $t = 0.2$ (before forming a shock) in Table 4. We also report the relative errors at $t = 1$ (after forming the shock) for the entropy-stable flux.

The numerical solutions converge to the reference RK4 solution with second-order accuracy for the MRK2, Relaxation-MRK2, and IDT-MRK2 methods regardless of the EC/ES fluxes at $t = 0.2$. The error differences among MRK2, Relaxation-MRK2, and IDT-MRK2 are within $\mathcal{O}(10^{-8})$. In particular, IDT-MRK2 shows second-order accuracy in time. This is because both Relaxation-MRK2 and IDT-MRK2 have tiny relaxation parameters ($\mathcal{O}(10^{-5})$), and the temporal error of IDT-MRK2 is not accumulated enough. This agrees with the previous study in [18, Figure 9.], where both IDT-RK2 and Relaxation-RK2 show the second-order rate of convergence in time. However, at $t = 1$, the error

(a) Total energy history (ES)
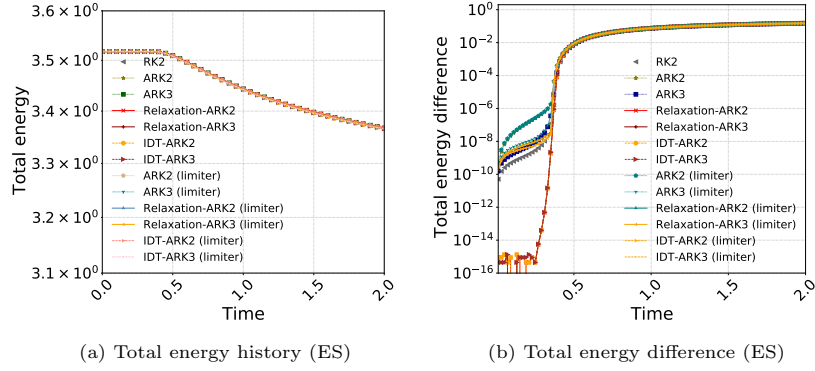
(b) Total energy difference (ES)

Figure 8: Gaussian example for the Burgers equation: histories of total energy and its difference with ES flux for ARK methods (standard, relaxation, and IDT). All the methods with ES flux show entropy-stable behaviors.
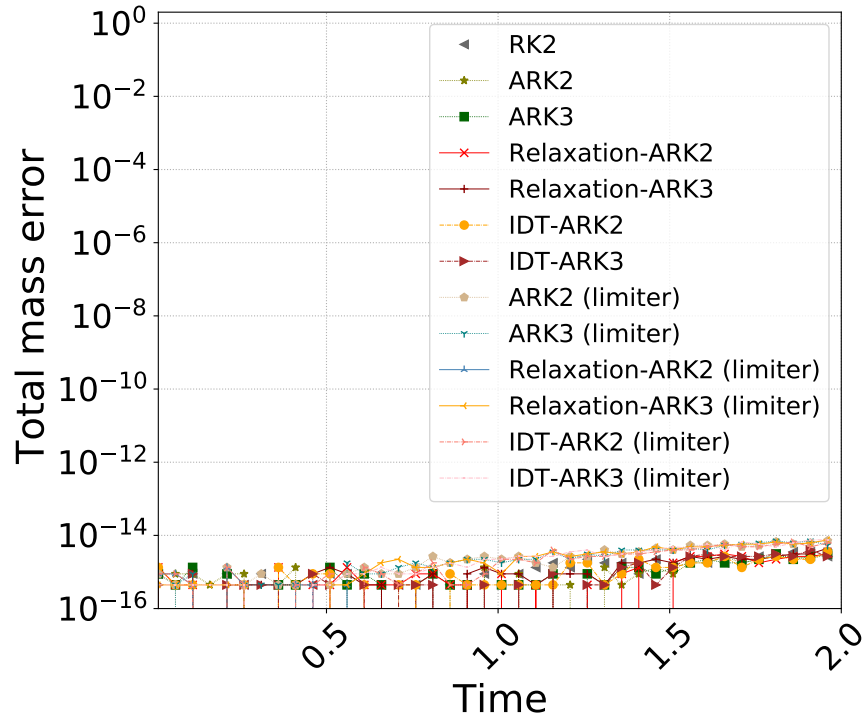

Figure 9: Histories of total mass difference of Gaussian example for the Burgers equation with ES flux: all the methods preserve the total mass within $\mathcal{O}(10^{-14})$ difference.
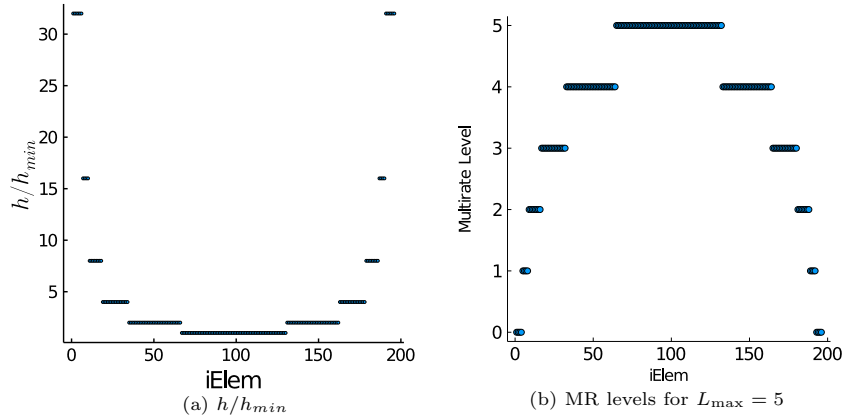
(a) h/h_{min}

(b) MR levels for $L_{\max} = 5$

Figure 10: (a) Ratio of element sizes with respect to the minimum size of the elements and (b) multirate levels of elements for $L_{\max} = 5$. Here, L is the maximum multirate (MR) level. The center of the domain is five times refined with a $2:1$ ratio so that the largest element is 32 times bigger than the smallest element. Multirate level is assigned to each element corresponding to the ratio of element sizes.

of IDT-MRK2 is at least sixty times larger than that of Relaxation-MRK2. We also observe that the order of temporal accuracy of IDT-MRK2 drops to one with larger time step sizes. The temporal error of IDT-MRK2 has accumulated to the point where the theoretical convergence rate can be seen. This agrees with Figure 7 where the location of the shock front for IDT-MRK2 is slightly behind that of Relaxation-MRK2.

Next, we examine the entropy conservation of MRK2 methods. We perform the simulations for $t \in [0, 2]$ with $N = 3$ and $K = 784$ ($L_{\max} = 5$). The time step size of RK2 is taken as $\triangle t_{RK} = 6.25 \times 10^{-6}$, whereas those of MRK2, Relaxation-MRK2, and IDT-MRK2 have $\triangle t = 20 \times \triangle t_{RK}$. [9] Figure 11 shows the time histories of the total energy and its difference for the RK2, MRK2, Relaxation-RK2, Relaxation-MRK2, IDT-RK2, and IDT-MRK2 methods. We see that both the relaxation and the IDT methods preserve the total energy during the simulation. The difference between the total energy for the relaxation and the IDT methods is around $\mathcal{O}(10^{-13})$, whereas the standard RK2 and MRK2 counterparts increase to $\mathcal{O}(10^{-1})$. We also show the snapshots at $t = 1$ in Figure 12. As expected, high oscillatory noises are observed, but numerical solutions are still stable.

Now we examine the entropy stability of MRK2 methods with ES flux. We perform the simulations for $t \in [0, 2]$ with $N = 3$ and $K = 784$ ($L_{\max} = 5$). The time step size of RK2 is taken as $\triangle t_{RK} = 5 \times 10^{-5}$, whereas the time step sizes of MRK2, Relaxation-MRK2, and IDT-MRK2 have $\triangle t = 25 \times \triangle t_{RK}$. [10] The snapshots at $t = 1$ are reported in Figure 13. Similar to Figure 7,

---

[9]RK2 with $\triangle t_{RK} = 1.25 \times 10^{-6}$ leads to blowup of its numerical solution.

[10]RK2 with $\triangle t_{RK} = 6.25 \times 10^{-5}$ yields a blowup solution.

26

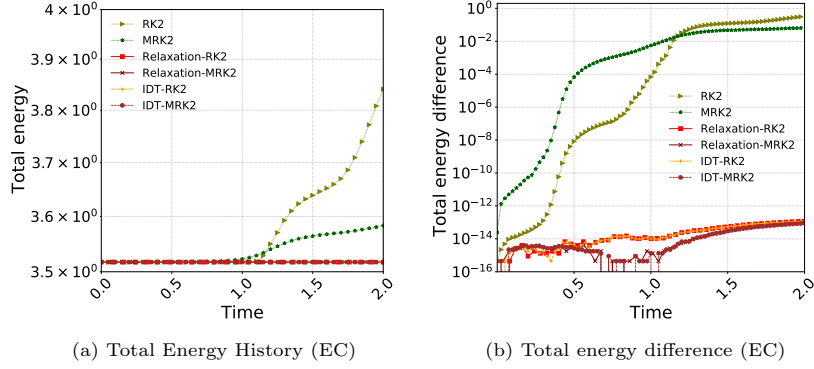(a) Total Energy History (EC)

(b) Total energy difference (EC)

Figure 11: Histories of total energy and its difference of Gaussian example for the Burgers equation with EC flux: the relaxation methods with EC flux conserve the total energy within $\mathcal{O}(10^{-13})$.
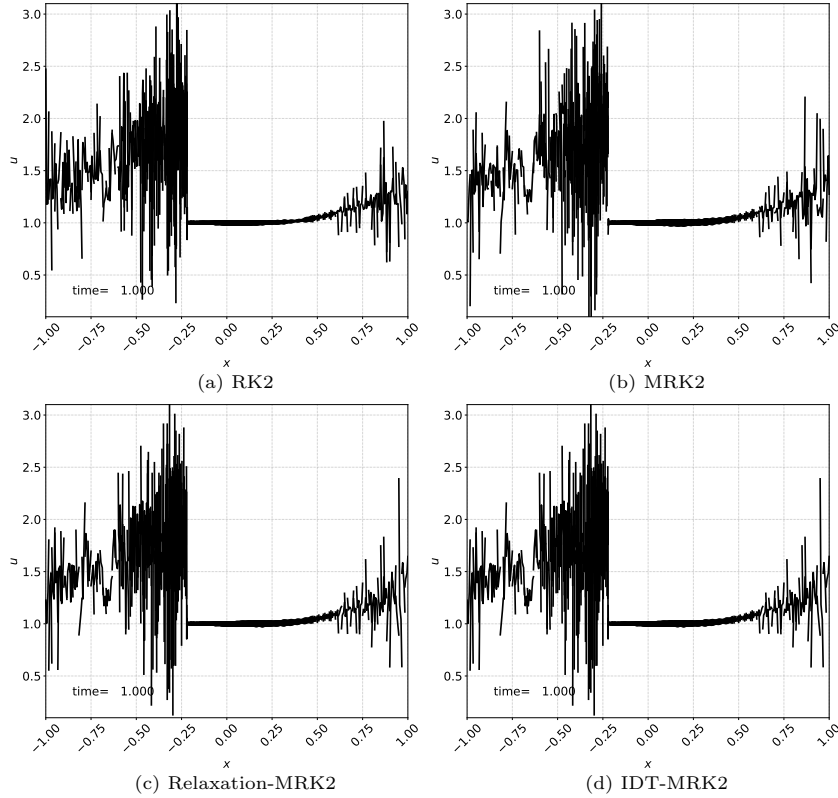

(a) RK2

(b) MRK2

(c) Relaxation-MRK2

(d) IDT-MRK2

Figure 12: Snapshots of Gaussian profile for the Burgers equation at $t = 1$ on a nonuniform mesh with energy-conserving (EC) flux for (a) RK2, (b) MRK2, (c) Relaxation-MRK2, and (d) IDT-MRK2. The time step size of RK2 is taken as $\triangle t_{RK} = 6.25 \times 10^{-6}$, whereas those of MRK2, Relaxation-MRK2, and IDT-MRK2 have $\triangle t = 20 \times \triangle t_{RK}$. The domain is discretized with a nonuniform mesh of $N = 3$ and $K = 784$ ($L_{\max} = 5$).

27

Table 4: Gaussian example: temporal convergence study for MRK2 methods performed with EC and ES fluxes on a nonuniform mesh of $N = 3$ and $K = 196$ without using the limiter. We use the time step sizes with $\triangle t = 0.001\,\{1, 1/2, 1/4, 1/8, 1/16\}$ for EC flux and $\triangle t = 0.0025\,\{1, 1/2, 1/4, 1/8, 1/16\}$ for ES flux. By taking the RK4 solution with the fixed step size of $\triangle t = 5.0 \times 10^{-6}$ as the "ground truth" solution, we measure the relative errors of MRK2, Relaxation-MRK2, and IDT-MRK2 methods at $t = 0.2$ (before forming a shock). We also report the relative errors at $t = 1.0$ (after forming the shock) for ES flux.

flux	$\triangle t$	MRK2		Relaxation-MRK2		IDT-MRK2	
		Error	Order	Error	Order	Error	Order
EC (t=0.2)	1.000e-03	5.67E-06	—	5.68E-06	—	5.59E-06	—
	5.000e-04	1.43E-06	1.98	1.43E-06	1.99	1.41E-06	1.98
	2.500e-04	3.61E-07	1.99	3.61E-07	1.99	3.56E-07	1.99
	1.250e-04	9.05E-08	2.00	9.06E-08	2.00	8.94E-08	1.99
	6.250e-05	2.27E-08	2.00	2.27E-08	2.00	2.24E-08	2.00
ES (t=0.2)	2.500e-03	7.43E-05	—	7.42E-05	—	9.22E-05	—
	1.250e-03	1.68E-05	2.14	1.68E-05	2.14	1.78E-05	2.37
	6.250e-04	4.02E-06	2.07	4.02E-06	2.07	4.04E-06	2.14
	3.125e-04	9.83E-07	2.03	9.83E-07	2.03	9.77E-07	2.05
	1.563e-04	2.43E-07	2.02	2.43E-07	2.02	2.41E-07	2.02
ES (t=1.0)	2.500e-03	1.46E-03	—	1.59E-03	—	9.68E-02	—
	1.250e-03	3.44E-04	2.08	3.01E-04	2.40	5.00E-02	0.95
	6.250e-04	8.35E-05	2.04	1.29E-04	1.22	1.36E-02	1.88
	3.125e-04	2.06E-05	2.02	2.25E-05	2.53	3.31E-03	2.04
	1.563e-04	5.11E-06	2.01	5.18E-06	2.12	8.22E-04	2.01

the IDT method suffers from phase errors. The shock front of IDT-MRK2 is slightly lagged behind, and the error becomes severe when the limiter is applied. This example demonstrates that the relaxation approach is better than the IDT approach in terms of accuracy, especially when the limiter is applied.

Figure 14 shows the time histories of the total entropy and its difference for the RK2, MRK2, Relaxation-RK2, Relaxation-MRK2, IDT-RK2, and IDT-MRK2 methods with/without the limiter. All the methods show entropy-stable behaviors. The entropy differences of all methods reach $\mathcal{O}(10^{-1})$ as time passes. In Figure 15 the time history of the total mass difference is shown for the RK2, MRK2, Relaxation-RK2, Relaxation-MRK2, IDT-RK2, and IDT-MRK2 methods with/without the limiter. In general, all the methods demonstrate good total mass conservation. In particular, without the limiter, all the methods preserve the total mass within $\mathcal{O}(10^{-14})$ error. With the limiter, however, the total mass difference is bounded by $\mathcal{O}(10^{-12})$ for the RK2, Relaxation-RK2, and IDT-RK2 methods and by $\mathcal{O}(10^{-13})$ for the MRK2, Relaxation-MRK2, and IDT-MRK2 methods.

(a) RK2

(b) RK2 w/ limiter

(c) MRK2

(d) MRK2 w/ limiter

(e) Relaxation-MRK2

(f) Relaxation-MRK2 w/ limiter

(g) IDT-MRK2
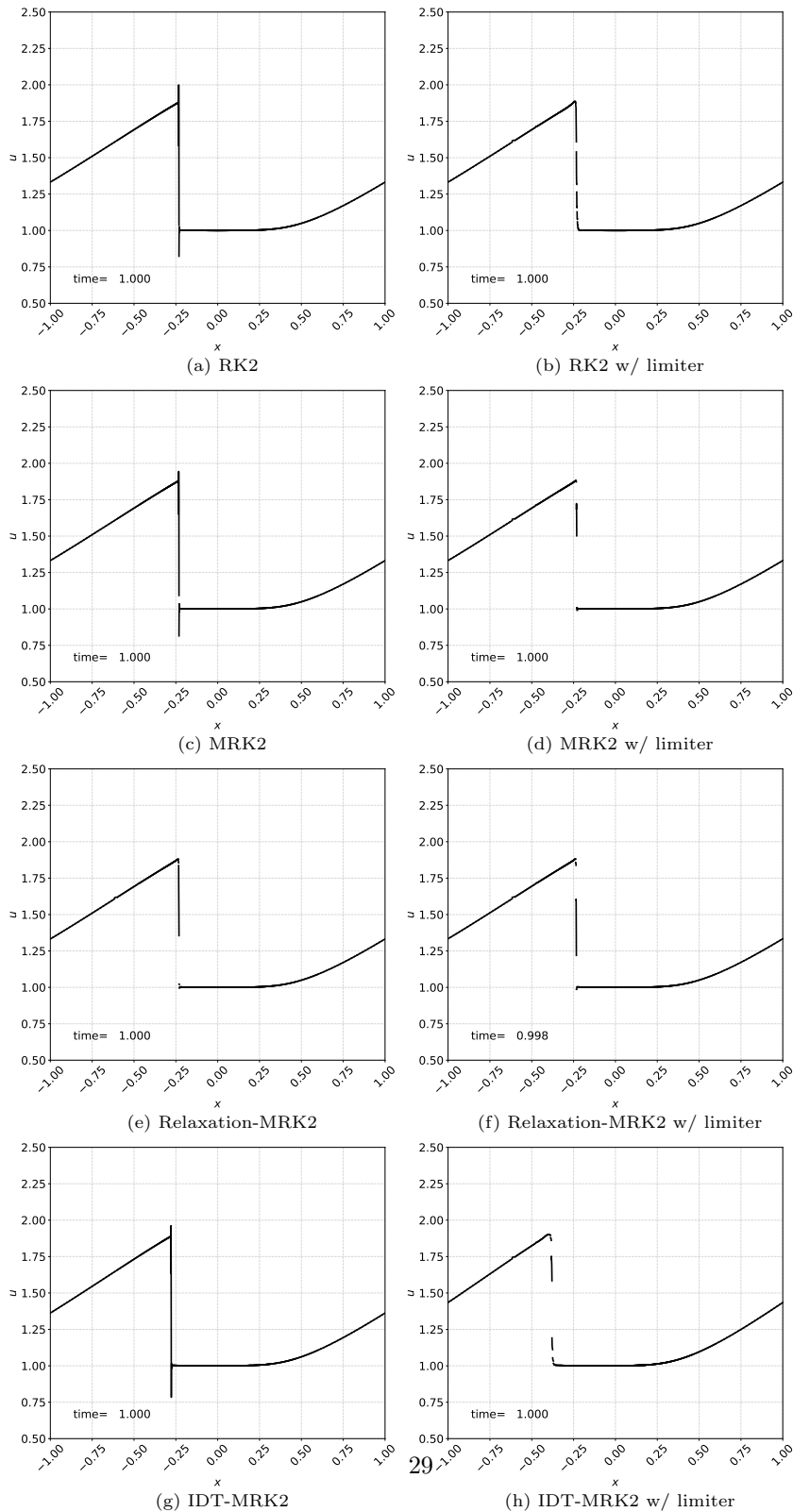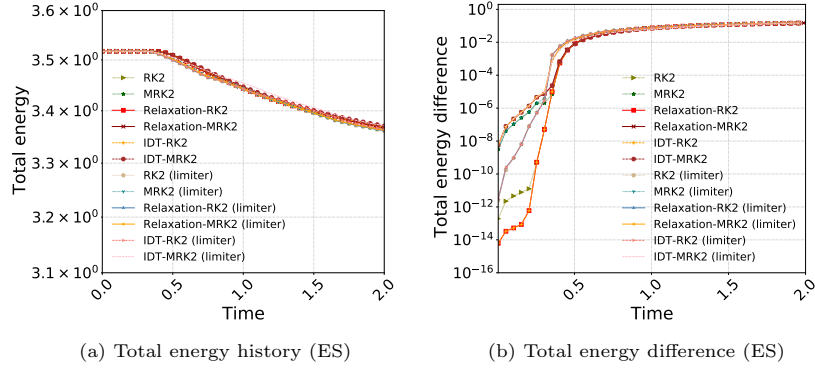
(h) IDT-MRK2 w/ limiter

Figure 13: Snapshots of Gaussian profile for the Burgers equation at $t = 1$ on a nonuniform mesh with entropy-stable (ES) flux for (a) RK2, (b) RK2 with limiter, (c) MRK2, (d) MRK2 with limiter, (e) Relaxation-MRK2, (f) Relaxation-MRK2 with limiter, (g) IDT-MRK2, and (h) IDT-MRK2 with limiter. The time step size of RK2 is taken as $\triangle t_{RK} = 5 \times 10^{-5}$, whereas those of MRK2, Relaxation-MRK2, and IDT-MRK2 have $\triangle t = 25 \times \triangle t_{RK}$. The domain is discretized with a nonuniform mesh of $N = 3$ and $K = 784$ ($L_{\max} = 5$).

(a) Total energy history (ES) (b) Total energy difference (ES)

Figure 14: Histories of total entropy and its difference of Gaussian example for the Burgers equation with ES flux: all the methods with ES flux show entropy-stable behaviors.
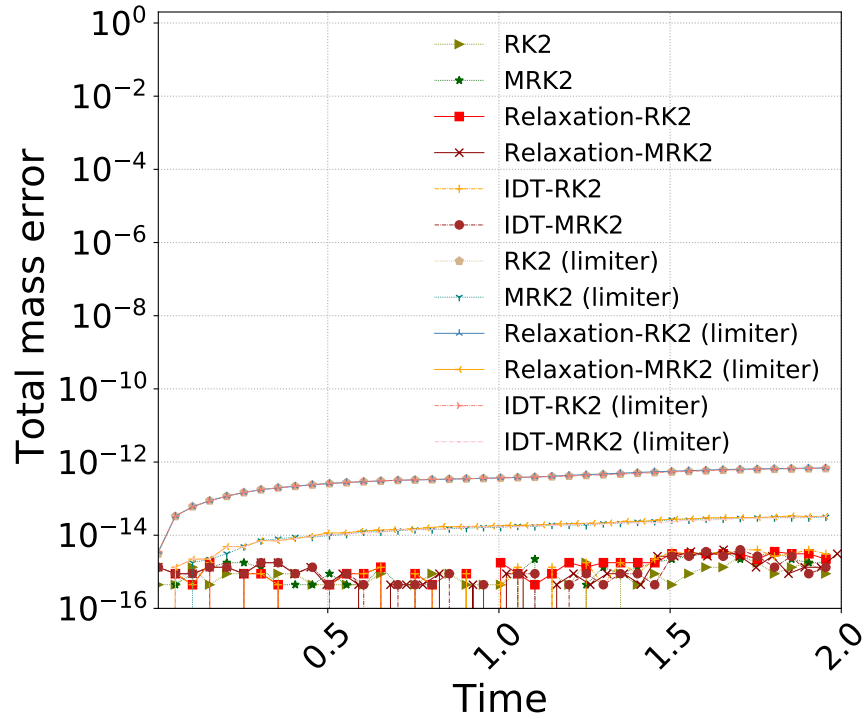
Figure 15: Histories of total mass difference of Gaussian example for the Burgers equation with ES flux: without the limiter, the methods preserve the total mass within $\mathcal{O}(10^{-14})$. However, the limiting procedure somehow affects the mass difference quantity, but the methods are bounded by $\mathcal{O}(10^{-12})$

(a) MR Levels   (b) Relaxation-MRK2
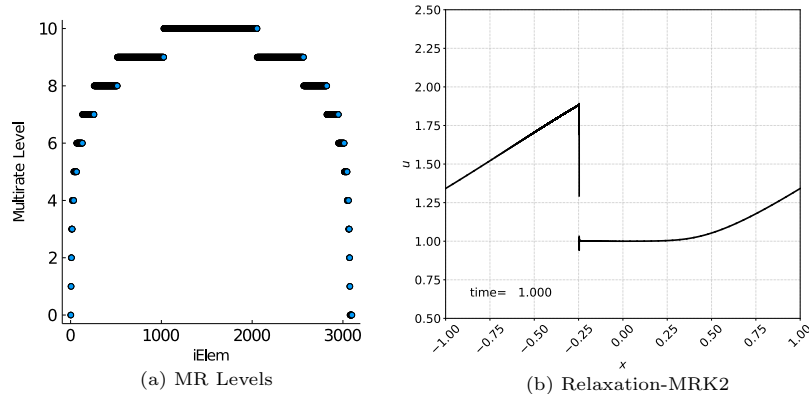
Figure 16: (a) Multirate levels of elements for $L_{\max} = 10$ and (b) snapshot of Gaussian profile for the Burgers equation at $t = 1$ on a nonuniform mesh with entropy-stable (ES) flux for Relaxation-MRK2. The domain is discretized with a nonuniform mesh of $N = 3$ and $K = 3099$.

We note that the relaxation approach in (20) is "global." The entropy conservation/stability in time is imposed only at the synchronization time for all steps, which corresponds to the coarsest time level. If numerical instability occurs during the stage integration of the multirate method, then the instability can lead to unstable numerical solutions. For this reason, when a shock occurs, we recommend using entropy-stable flux rather than entropy-conserving flux because the diffusive penalty term in entropy-stable flux helps mitigate the numerical instability. Indeed, we numerically observed that the relaxation approach is stable with entropy-stable flux on deeply nested mesh refinement. We perform a numerical simulation for $t \in [0, 1]$ with $\triangle t = 0.002$. The computational domain is non-uniformly refined with $L_{\max} = 10$, $N = 3$, and $N_E = 3099$. Figure 16 shows the snapshot of Gaussian example at $t = 1$ without the limiter. The shock front is highly resolved thanks to the fine resolution, and hence sharp spikes at the shock front are reduced, compared with Figure 13e.

4. Conclusions

In this paper we present entropy-preserving/stable time discretization methods for partitioned Runge–Kutta schemes. Our work is an extension of the explicit relaxation Runge–Kutta methods [18, 21] to partitioned Runge–Kutta methods. In particular, we use the relaxation method to IMEX–RK methods and to a class of explicit second-order multirate methods. IMEX-RK methods allow for a longer time step size than that restricted by explicit methods by defining the linearized flux containing the fast wave in the system with the stiffness being implicitly treated. Multirate methods decompose the original problem into subproblems, where different time step sizes can be used locally on each subproblem. Unlike IMEX-RK methods, multirate methods do not require any linear/nonlinear solve and, hence, are attractive for parallel computing

if proper preconditioning is not available. In combination with entropy conservation/stable spatial discretization, the proposed method successfully demonstrates the entropy conservation and stability properties for a few ODEs and the Burgers equation.

We numerically found that Relaxation-ARK approaches provide high-order accuracy in time, whereas the Relaxation-MRK2 method has a second-order rate of convergence, as expected. We also observed that the relaxation approach is one degree more accurate than the incremental direction technique when enough temporal errors have accumulated. The location error of the incremental direction technique is larger than the relaxation strategy, especially in the presence of shocks. When the limiter is used, the inaccuracy becomes substantially worse. However, regardless of whether or not the limiter is applied, all the Relaxation-ARK, Relaxation-MRK2, IDT-ARK, IDT-MRK2 methods show entropy-conserving/stable behavior for the Burgers equation.

The key idea of the relaxation method is to adjust the step completion with the relaxation parameter so that the time-adjusted solution satisfies entropy conservation and stability properties. The relaxation parameter is computed by solving a scalar nonlinear equation in general at each timestep; but, as for energy entropy, the relaxation parameter can be determined explicitly. We theoretically provided the explicit forms of the relaxation parameters for IMEX-RK methods and the multirate methods and numerically verified that the explicit relaxation parameters work for the Burgers equation.

We note that entropy conservation/stability in time is guaranteed only at the coarsest time level. Numerical solutions may become unstable if numerical instability arises during the stage integration of the IMEX or multirate methods. Because of the implicit correction step at each stage, Relaxation-ARK approaches can reduce numerical instability. Relaxation-MRK2, on the other hand, lacks the ability to manage instability during stage integration. Therefore, with Relaxation-MRK2, entropy-stable flux is preferred above entropy-conserving flux, especially on deep-nested mesh refinement. We showed that Relaxation-MRK2 with entropy-stable flux performs well on the deep-nested mesh refinement (with 10 levels).

To exploit more sophisticated problems, we will focus our future work on extension to multidimensions as well as additional partial differential equations, such as Euler equations. Working on entropy-conserving/entropy-stable coupling techniques for multiphysics problems is also interesting.

Acknowledgments

Declaration

Availability of data and material

The datasets generated during and/or analyzed during the current study are available from the corresponding author on reasonable request.

Code availability

The code used to generate the results is available from the corresponding author on reasonable request.

[1] M. Ainsworth, Dispersive and dissipative behaviour of high order discontinuous Galerkin finite element methods, Journal of Computational Physics 198 (1) (2004) 106–130.

[2] J. Chan, On discretely entropy conservative and entropy stable discontinuous Galerkin methods, Journal of Computational Physics 362 (2018) 346–374.

[3] E. Tadmor, The numerical viscosity of entropy stable schemes for systems of conservation laws. I, Mathematics of Computation 49 (179) (1987) 91–103.

[4] G. S. Jiang, C.-W. Shu, On a cell entropy inequality for discontinuous Galerkin methods, Mathematics of Computation 62 (206) (1994) 531–538.

[5] J. Nordström, M. Svärd, Well-posed boundary conditions for the Navier–Stokes equations, SIAM Journal on Numerical Analysis 43 (3) (2005) 1231–1255.

[6] U. S. Fjordholm, S. Mishra, E. Tadmor, Arbitrarily high-order accurate entropy stable essentially nonoscillatory schemes for systems of conservation laws, SIAM Journal on Numerical Analysis 50 (2) (2012) 544–573.

[7] T. C. Fisher, M. H. Carpenter, High-order entropy stable finite difference schemes for nonlinear conservation laws: Finite domains, Journal of Computational Physics 252 (2013) 518–557.

[8] G. J. Gassner, A skew-symmetric discontinuous Galerkin spectral element discretization and its relation to SBP-SAT finite difference methods, SIAM Journal on Scientific Computing 35 (3) (2013) A1233–A1253.

[9] M. H. Carpenter, T. C. Fisher, E. J. Nielsen, S. H. Frankel, Entropy stable spectral collocation schemes for the Navier–Stokes equations: Discontinuous interfaces, SIAM Journal on Scientific Computing 36 (5) (2014) B835–B867.

[10] D. C. D. R. Fernández, P. D. Boom, D. W. Zingg, A generalized framework for nodal first derivative summation-by-parts operators, Journal of Computational Physics 266 (2014) 214–239.

[11] G. J. Gassner, A. R. Winters, D. A. Kopriva, Split form nodal discontinuous Galerkin schemes with summation-by-parts property for the compressible Euler equations, Journal of Computational Physics 327 (2016) 39–66.

[12] N. Wintermeyer, A. R. Winters, G. J. Gassner, D. A. Kopriva, An entropy stable nodal discontinuous Galerkin method for the two dimensional shallow water equations on unstructured curvilinear meshes with discontinuous bathymetry, Journal of Computational Physics 340 (2017) 200–242.

[13] T. Chen, C.-W. Shu, Entropy stable high order discontinuous Galerkin methods with suitable quadrature rules for hyperbolic conservation laws, Journal of Computational Physics 345 (2017) 427–461.

[14] J. Nordström, T. Lundquist, Summation-by-parts in time, Journal of Computational Physics 251 (2013) 487–499.

[15] P. D. Boom, D. W. Zingg, High-order implicit time-marching methods based on generalized summation-by-parts operators, SIAM Journal on Scientific Computing 37 (6) (2015) A2682–A2709.

[16] H. Ranocha, J. Nordström, A new class of a stable summation by parts time integration schemes with strong initial conditions, Journal of Scientific Computing 87 (1) (2021) 1–25.

[17] L. Friedrich, G. Schnücke, A. R. Winters, D. C. D. R. Fernández, G. J. Gassner, M. H. Carpenter, Entropy stable space–time discontinuous Galerkin schemes with summation-by-parts property for hyperbolic conservation laws, Journal of Scientific Computing 80 (1) (2019) 175–222.

[18] D. I. Ketcheson, Relaxation Runge–Kutta methods: Conservation and stability for inner-product norms, SIAM Journal on Numerical Analysis 57 (6) (2019) 2850–2870.

[19] J. Sanz-Serna, An explicit finite-difference scheme with exact conservation properties, Journal of Computational Physics 47 (2) (1982) 199–210.

[20] J. Sanz-Serna, V. Manoranjan, A method for the integration in time of certain partial differential equations, Journal of Computational Physics 52 (2) (1983) 273–289.

[21] H. Ranocha, L. Lóczi, D. I. Ketcheson, General relaxation methods for initial-value problems with application to multistep schemes, Numerische Mathematik 146 (4) (2020) 875–906.

[22] R. Abgrall, E. L. Mélédo, P. Öffner, D. Torlo, Relaxation deferred correction methods and their applications to residual distribution schemes, arXiv preprint arXiv:2106.05005 (2021).

[23] H. Ranocha, D. I. Ketcheson, Relaxation Runge–Kutta methods for Hamiltonian problems, Journal of Scientific Computing 84 (1) (2020) 1–27.

[24] H. Ranocha, M. Sayyari, L. Dalcin, M. Parsani, D. I. Ketcheson, Relaxation Runge–Kutta methods: Fully discrete explicit entropy-stable schemes for the compressible Euler and Navier–Stokes equations, SIAM Journal on Scientific Computing 42 (2) (2020) A612–A638.

[25] E. M. Constantinescu, A. Sandu, Multirate timestepping methods for hyperbolic conservation laws, Journal of Scientific Computing 33 (3) (2007) 239–278.

[26] C. P. Stone, R. L. Davis, Techniques for solving stiff chemical kinetics on graphical processing units, Journal of Propulsion and Power 29 (4) (2013) 764–773.

[27] Y. Komori, K. Burrage, A stochastic exponential euler scheme for simulation of stiff biochemical reaction systems, BIT Numerical Mathematics 54 (4) (2014) 1067–1085.

[28] A. Bartel, M. Günther, A. Kværnø, Multirate methods in electrical circuit simulation, in: Progress in Industrial Mathematics at ECMI 2000, Springer, 2002, pp. 258–265.

[29] S. Kang, F. X. Giraldo, T. Bui-Thanh, IMEX HDG-DG: A coupled implicit hybridized discontinuous Galerkin and explicit discontinuous Galerkin approach for shallow water systems, Journal of Computational Physics (2019) 109010.

[30] U. M. Ascher, S. J. Ruuth, R. J. Spiteri, Implicit-explicit Runge-Kutta methods for time-dependent partial differential equations, Applied Numerical Mathematics 25 (2) (1997) 151–167.

[31] F. X. Giraldo, M. Restelli, M. Läuter, Semi-implicit formulations of the Navier–Stokes equations: Application to nonhydrostatic atmospheric modeling, SIAM Journal on Scientific Computing 32 (6) (2010) 3394–3425.

[32] D. J. Gardner, J. E. Guerra, F. P. Hamon, D. R. Reynolds, P. A. Ullrich, C. S. Woodward, Implicit–explicit (IMEX) Runge–Kutta methods for nonhydrostatic atmospheric models, Geoscientific Model Development 11 (4) (2018) 1497–1515.

[33] C. Newman, G. Womeldorff, D. A. Knoll, L. Chacón, A communication-avoiding implicit–explicit method for a free-surface ocean model, Journal of Computational Physics 305 (2016) 877–894.

[34] J.-F. Lemieux, D. A. Knoll, M. Losch, C. Girard, A second-order accurate in time implicit–explicit (IMEX) integration scheme for sea ice dynamics, Journal of Computational Physics 263 (2014) 375–392.

[35] S. Streiner, S. Hauptmann, M. Kühn, E. Krämer, Coupled fluid-structure simulations of a wind turbine rotor, in: Deutsche Windenergie-Konferenz (DEWEK), Bremen, Germany, DEWI-German Wind Energy Institute, 2008.

[36] S. T. Miller, E. C. Cyr, J. N. Shadid, R. M. J. Kramer, E. G. Phillips, S. Conde, R. P. Pawlowski, IMEX and exact sequence discretization of the multi-fluid plasma model, Journal of Computational Physics 397 (2019) 108806.

[37] A. Kanevsky, M. H. Carpenter, D. Gottlieb, J. S. Hesthaven, Application of implicit–explicit high–order Runge–Kutta methods to discontinuous Galerkin schemes, Journal of Computational Physics 225 (2) (2007) 1753–1781.

[38] W. C. Skamarock, J. B. Klemp, A time-split nonhydrostatic atmospheric model for weather research and forecasting applications, Journal of Computational Physics 227 (7) (2008) 3465–3485.

[39] B. Seny, J. Lambrechts, R. Comblen, V. Legat, J.-F. Remacle, Multirate time stepping for accelerating explicit discontinuous Galerkin computations with application to geophysical flows, International Journal for Numerical Methods in Fluids 71 (1) (2013) 41–64.

[40] M. Schlegel, O. Knoth, M. Arnold, R. Wolke, Implementation of multirate time integration methods for air pollution modelling, Geoscientific Model Development 5 (6) (2012) 1395–1405.

[41] J. Wensch, O. Knoth, A. Galant, Multirate infinitesimal step methods for atmospheric flow simulation, BIT Numerical Mathematics 49 (2) (2009) 449–473.

[42] C. Mikida, A. Klöckner, D. Bodony, Multi-rate time integration on overset meshes, Journal of Computational Physics 396 (2019) 325–346.

[43] M. H. Carpenter, T. C. Fisher, High-order entropy stable formulations for computational fluid dynamics, in: 21st AIAA Computational Fluid Dynamics Conference, 2013, p. 2868.

[44] M. Calvo, D. Hernández-Abreu, J. I. Montijano, L. Rández, On the preservation of invariants by explicit Runge–Kutta methods, SIAM Journal on Scientific Computing 28 (3) (2006) 868–885.

[45] L. Pareschi, G. Russo, Implicit-explicit Runge-Kutta schemes and applications to hyperbolic systems with relaxation, Journal of Scientific computing 25 (1-2) (2005) 129–155.

[46] C. A. Kennedy, M. H. Carpenter, Additive Runge-Kutta schemes for convection-diffusion-reaction equations, Applied Numerical Mathematics 44 (1-2) (2003) 139–181.

[47] F. X. Giraldo, J. F. Kelly, E. Constantinescu, Implicit-explicit formulations of a three-dimensional nonhydrostatic unified model of the atmosphere (NUMA), SIAM Journal on Scientific Computing 35 (5) (2013) B1162–B1194.

[48] C.-W. Shu, S. Osher, Efficient implementation of essentially non-oscillatory shock-capturing schemes, Journal of computational physics 77 (2) (1988) 439–471.

[49] F. X. Giraldo, J. F. Kelly, E. M. Constantinescu, Implicit-explicit formulations of a three-dimensional nonhydrostatic unified model of the atmosphere (NUMA), SIAM Journal on Scientific Computing 35 (5) (2013) B1162–B1194.